Competitive nitrogen versus carbon tunneling

Cláudio M. Nunes,[1]* André K. Eckhardt,[2] Igor Reva,[1] Rui Fausto,[1] Peter R. Schreiner[2]*

[1]CQC, Department of Chemistry, University of Coimbra, 3004-535 Coimbra, Portugal.

[2]Institute of Organic Chemistry, Justus Liebig University, Heinrich-Buff-Ring 17, 35392 Giessen, Germany.

ABSTRACT: Quantum mechanical tunneling (QMT) of heavy atoms like carbon or nitrogen for the longest time has been considered very unlikely, but recent evidence suggests that heavy-atom QMT does occur more frequently than assumed. Here we demonstrate that carbon vs. nitrogen heavy-atom QMT can even be competitive leading to two different products originating from the *same* starting material. Amino-substituted benzazirine was generated in solid argon (3–18 K) and found to decay spontaneously in the dark, with a half-life time of 210 min, to *p*-aminophenylnitrene and amino-substituted ketenimine. The reaction rate is independent of the cryogenic temperature, in contradiction with the rules defined by classical transition state theory. Quantum chemical computations confirm the existence of two competitive carbon vs. nitrogen QMT reaction pathways. This discovery emphasizes that the quantum nature of atoms and molecules, thereby enabling a much higher level of control and a deeper understanding of the factors that govern chemical reactivity.

INTRODUCTION

Quantum mechanical tunneling (QMT) is a fascinating phenomenon with serious implications for physics, chemistry, and the life sciences.[1-11] Still, it has not found firm entry into the latter two disciplines, in particular, not into reaction planning that is overwhelmingly governed by assuming classic (hard sphere particle) behavior of all atoms involved in chemical transformations. Apart from ignoring the quantum nature of atoms and molecules, this leaves out a wealth of information and opportunities for discovering novel chemical transformations. QMT is a consequence of the wave-particle duality and manifests itself in reactions occurring with atomic nuclei moving distances comparable to their de Broglie wavelengths. In this situation, there is a finite probability of finding an atomic nucleus on the other side of a potential energy barrier, even when the system possesses insufficient energy to surmount it. QMT is more common for light nuclei, in particular, hydrogen atoms (or ions), but it is by no means limited to these. However, because tunneling probabilities decrease exponentially with the square root of the moving mass,[12] direct experimental observation of heavy-atom QMT is very rare.[13-21] Here we demonstrate that heavy-atom QMT can even be competitive, thereby yielding different products originating from the same starting material. As we will show, classical transition state theory (TST) is not able to predict the outcome of the reaction in the studied chemical system, competitive QMT determines all reactivity at the cryogenic temperatures of the experiments.

Signatures of QMT in chemical reactions have been often obtained indirectly, typically by the observation of exceptionally large kinetic isotope effects (KIEs) and non-linear Arrhenius plots.[2,4,22] Direct spectroscopic evidence of a variety of tunneling reactions has been provided using low-temperature matrix-isolation techniques, particularly during the last decade.[7,23] Owing to the very little thermal energy available, reactions observed under cryogenic conditions (usually 3–12 K) occur mostly due to tunneling, and are therefore easily recognizable.[24] Tunneling can also occur at ambient temperatures[4,25] but it is normally accompanied by the thermal over-the-barrier reactivity, whose relative importance increases significantly with temperature. Investigations at cryogenic temperatures have contributed significantly to a better understanding of the role and prevalence of QMT in chemistry and to the discovery of new reactivity paradigms.[23] Particularly exciting was the discovery of *tunneling control* of chemical reactions, i.e., tunneling reactions that lead exclusively to a product whose reaction path faces a higher barrier, superseding kinetic control and breaking the rules inferred from TST.[26] Other surprising observations include the discovery of a tunneling product that is neither thermodynamically nor kinetically favored and a conformer-specific tunneling reaction where the Curtin-Hammett principle is not applicable.[27-29]

Some of us have been involved in exploring the potential energy surface (PES) of aryl nitrenes **2** (Scheme 1). Such species are very reactive and short-lived intermediates, usually generated by decomposition of aryl azides **1**, having applications in photoresists, photoaffinity labelling, and as building blocks for the preparation of materials as well as organic molecules.[30-32]

Scheme 1. PES of Aryl Nitrenes Illustrated by the Example of Parent Phenylnitrene 2a.[a]

$^1A_2$ (−4.1)
$^3A_2$ (−22.6)
(0.0)
(−5.7)
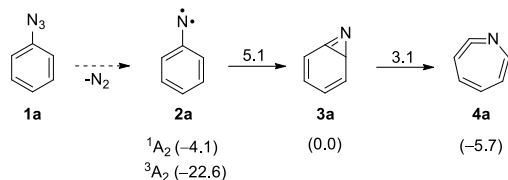
[a]Relative energies (in kcal mol⁻¹) of minima (in parentheses) and transitions states (above the arrows) involved in the isomerization of **2a** computed at the CASPT2N(8,8)/6-311G(2d,p)//CASSCF(8,8)/6-31G(d) level of theory.[33] $^1A_2$ = open-shell singlet state, $^3A_2$ = triplet ground state.

Although research on aryl nitrenes is a mature field, with more than 50 years of literature reports, their slippery and electronically intricate PESs are still fascinating. For instance, recent studies unraveled novel examples of H-atom and heavy-atom QMT on the PES of 2-formylphenylnitrene **2b**,[19,34] namely the H-atom tunneling from the corresponding aryl nitrene **2b** to imino ketene **5b** and the heavy-atom tunneling rearrangement of the corresponding benzazirine **3b** to the cyclic ketenimine **4b** (Scheme 2).

Scheme 2. Top: H-Atom Tunneling of Triplet 2-Formyl-phenylnitrene ³2b to Imino-Ketene 5b.[34] **Bottom: Heavy-Atom Tunneling of Benzazirine 3b to Ketenimine 4b.**[19]
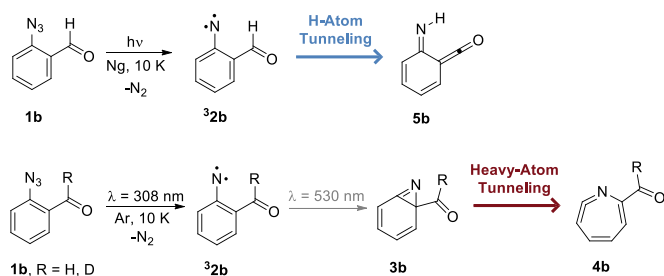
Benzazirines **3**, formed upon cyclization of aryl nitrenes **2**, are highly elusive species as they are typically higher in energy than **2** (both the triplet ground state ($^3A_2$) and the first excited open-shell singlet state ($^1A_2$)) and are separated by a low energy barrier from decaying to cyclic ketenimines **4**.[31,35] Multiconfigurational computations on the PES of parent phenylnitrene **2a** estimate an energy barrier for ring expansion of benzazirine **3a** to cyclic ketenimine **4a** of only ~3 kcal mol⁻¹ (Scheme 1).[33] Actually, parent **3a** still remains elusive, and only very few benzazirine derivatives have been characterized under cryogenic conditions.[36,37] Recent evidence suggests that heavy-atom tunneling contributes to turn **3** into a fleetingly existent species, even at very low temperatures.[17,19,38] It appears that in order to capture derivatives of **3** at cryogenic temperatures and prevent tunneling reactions to occur the energy barrier to **4** needs to be significantly higher than that for the parent species. Computations predict that *para*-substituted electron-donating groups (EDGs) increase the energy barrier for

the ring expansion of **3** to **4** so that this step becomes rate-determining in the isomerization process of **2** to **4**.[39,40] Therefore, we envisaged that *para*-EDG-substituted **2** would provide access to **3**. Here, we investigated the PES of *p*-aminophenylnitrene **2c** and the role QMT plays with respect to rearrangement reactions of **3c** to the thermodynamically more stable products **2c** and **4c** (Scheme 3). This led us to discover a new reactivity paradigm, the occurrence of two competitive tunneling reactions originating from the same chemical species.

Scheme 3. Summary of Light Induced and Tunneling Reactivity in Argon Matrices at 3 K on the PES of *p*-Aminophenylnitrene 2c.
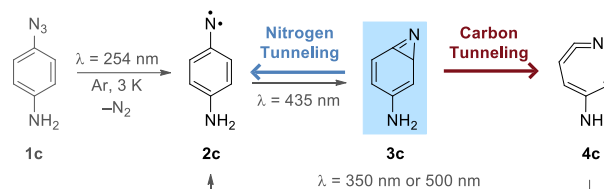
RESULTS AND DISCUSSION

Light induced reactivity and characterization. Azide **1c** was irradiated with $\lambda = 254$ nm in an argon matrix at 3 K (Figure S1, Supporting Information) to produce triplet nitrene $^3A_2$-**2c** and a small amount of ketenimine **4c** (Figure 1).[41] The longer the irradiation time, the lower the $^3A_2$-**2c**:**4c** ratio, indicating that **4c** most probably forms through a secondary photoreaction of $^3A_2$-**2c**. Both photoproducts can be made to react selectivity by subsequent UV excitation at different wavelengths.
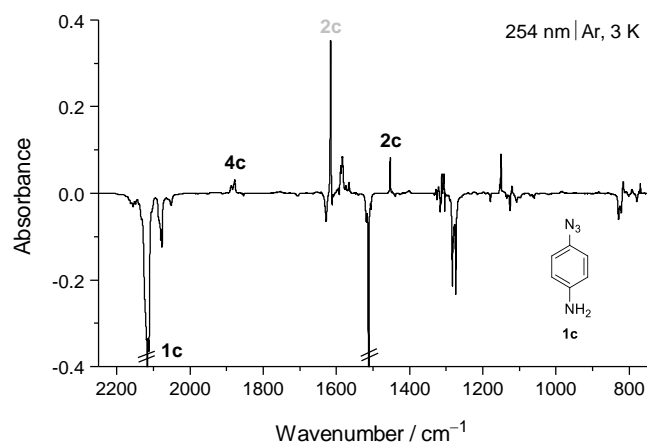

Figure 1. Experimental difference IR spectrum obtained as the spectrum after irradiation at $\lambda = 254$ nm (16 min) of *p*-azidoaniline **1c** isolated in an argon matrix at 3 K "minus" the spectrum of the sample before irradiation. The negative bands are due to the consumed **1c**. The positive bands labeled as **2c** (1453 cm^{-1}) and **4c** (1887/1878 cm^{-1}) are the most characteristic stand-alone bands of the generated products. The most intense band appearing at 1616 cm^{-1} has a major contribution of photoproduct $^3A_2$-**2c** and a small contribution of photoproduct **4c**, which are partially overlapped with each other. By this reason the assignment is shown in gray color.

Species **4c** can be selectively converted to $^3A_2$-**2c** by irradiation at $\lambda = 350$ nm. The depleted bands in the experimental difference infrared (IR) spectrum show a clear correspondence with the IR spectrum of **4c** computed at the B3LYP/6-311+G(2d,p) level of theory (Figure 2). Representative are the experimental bands observed at 1887/1878, 1624/1608, 1590, 1199, 1106, 986/982, and 792 cm^{-1}, which are in good agreement with the computed characteristic bands of **4c** at 1896 [ν_{as}(C=C=N)], 1625 [δ(NH$_2$)], 1590 [ν_{as}(C=C)], 1195 [ν(C–NH$_2$)], 1115 [ν_s(C=C=N)], 985 [ν(C–NC)], and 793 [γ(CH)] cm^{-1} (additional data are provided in Table S2). Concomitantly with the depletion of **4c**, a set of new IR bands arises that compares very well with the computed IR spectrum of $^3A_2$-**2c**. The most intense experimental bands are observed at 1616, 1588/1584, 1453, 1312, 1308/1306, 1154/1151, and 817/807 cm^{-1}, which nicely match the computed most intense bands of $^3A_2$-**2c** at 1623 [δ(NH$_2$)], 1586 [ν_{ring1}(CC)], 1452 [ν_{ring3}(CC) – ν(C–NH$_2$)], 1305 [ν(C–N)], 1292 [ν(C–NH$_2$) + ν_{ring3}(CC)], 1150 [δ(CH)], and

807 [γ(CH)] cm^{-1} (see also Table S3). Ketenimine **4c** was also selectively converted to $^3A_2$-**2c** using narrowband irradiation at $\lambda = 500$ nm (or slightly shorter wavelengths) provided by a laser-OPO system. The result suggests that **4c** has a very weak and broad absorption band extending up to this wavelength. The UV-vis spectroscopic characterization of these species is presented and discussed in the Supporting Information, Section 1.
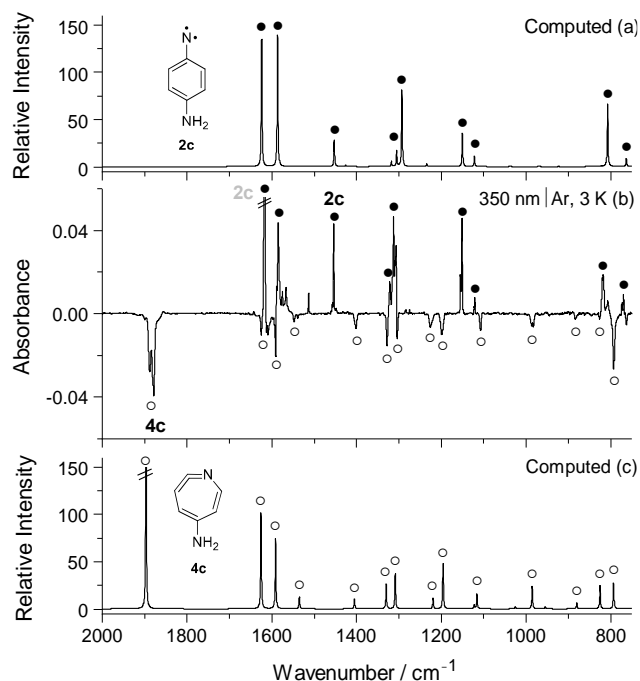

Figure 2. (a) IR spectrum of triplet *p*-aminophenylnitrene $^3A_2$-**2c** computed at the B3LYP/6-311+G(2d,p) level of theory. (b) Experimental difference IR spectrum showing changes after irradiation at $\lambda = 350$ nm (8 min; argon matrix at 3 K), subsequent to irradiation at $\lambda = 254$ nm (Figure 1). The downward bands are due to consumed species assigned to **4c**. The upward bands are due to the produced species assigned to $^3A_2$-**2c**. (c) IR spectrum of amino-substituted ketenimine **4c** computed at B3LYP/6-311+G(2d,p) level of theory.

The depletion of nitrene $^3A_2$-**2c** can be achieved upon irradiation at $\lambda = 435$ nm, resulting in the formation of **4c** and a small amount of **3c** (Figure S4). Ketenimine **4c** was readily spotted by the characteristic strong ν_{as}(C=C=N) absorption at 1887/1878 cm^{-1} and its entire IR spectral signature was identified by comparison with data shown in Figure 2. The additionally observed weak IR bands, which were not assigned to **4c**, were assigned to the benzazirine **3c**. The most characteristic bands of **3c** are observed at 1710, 1508/1503, 1403, and 1246 cm^{-1}, in good agreement with the most intense bands of this species computed at 1746 [ν(C=N)], 1497 [ν_s(C=C)], 1407 [δ(CH)], and 1229 [ν(C–NH$_2$)] cm^{-1}. The slight overestimation of ν(C=N) of **3c** (~36 cm^{-1}) is consistent with the B3LYP computed IR spectra of other benzazirines (Table S4).[19] Moreover, as discussed in the next section, we found that

3

3c spontaneously rearranges in cryogenic noble gas matrices. Thus, a clearer and more complete IR spectral signature was obtained for this species. As shown in Figure 3, the excellent match between the experimental and the B3LYP/6-311+G(2d,p) computed IR spectra provides strong evidence to unequivocally establish the first IR-spectroscopic identification of **3c**. A detailed assignment of the IR spectrum of **3c** (a total of 19 experimental bands) is given in Table S5.
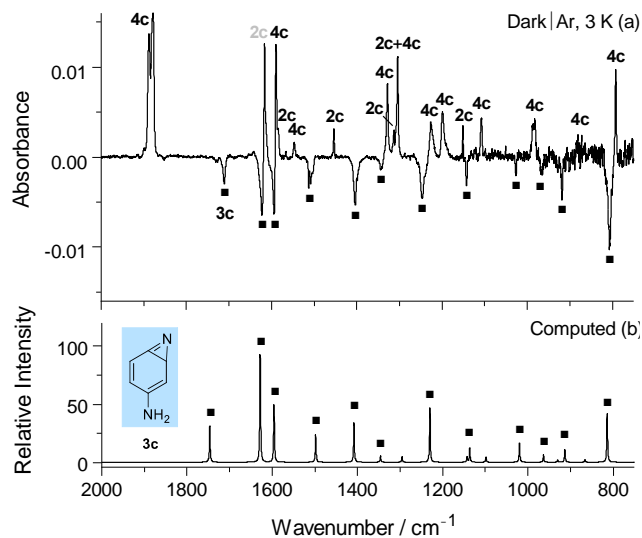

Figure 3. (a) Experimental difference IR spectrum showing changes after keeping the sample at 3 K (argon matrix) in the dark for 24 h, subsequent to irradiation at λ = 435 nm (Figure S4). The downward bands are due to the consumption of **3c**. The upward bands arise from the formation of both ³A₂-**2c** and **4c**. (b) IR spectrum of amino-substituted benzazirine **3c** computed at B3LYP/6-311+G(2d,p) level of theory.

Tunneling reactivity. Benzazirine **3c** is metastable under matrix-isolation conditions. In an argon matrix at temperatures as low as 3 K and in the dark (the sample was protected from the IR spectrometer globar source), **3c** spontaneously rearranges to give two products, namely triplet nitrene ³A₂-**2c** and singlet ketenimine **4c** (Figure 3). The formation of ³A₂-**2c** and **4c** is readily identified by their most intense bands in accordance with data shown in Figure 2 (see also Tables S2 and S3). To minimize the effect of the IR spectrometer light, kinetic measurements were performed by collecting only a few spectra (using a cutoff filter below 2200 cm^{-1}) over long time intervals (Figure 4). Although the kinetics of the spontaneous rearrangement of **3c** shows some dispersive character,[42] for the sake of simplification, the data were fitted with an equation of single-exponential decay, giving an estimated rate constant (k_3) of ~5.5 × 10^{-5} s^{-1}, corresponding to a half-life time ($t_{1/2}$) of ~210 min (Figure S6). The ³A₂-**2c**:**4c** ratio is roughly 15:85. Therefore, considering a competing unidirectional first-order reaction of a single reactant to give two different products, the rate constants k_2 and k_4, corresponding to the formation of ³A₂-**2c** and **4c**, are estimated to be ~8.3 × 10^{-6} s^{-1} ($t_{1/2}$ ~1400 min) and ~4.7 × 10^{-5} s^{-1} ($t_{1/2}$ ~ 247 min), respectively (see Experimental and Computational Methods section for details).

To determine whether the spontaneous rearrangement of **3c** is thermally activated as in an over-the-barrier process, additional experiments were carried out at higher temperatures (3 – 18 K). Using an approach similar to that described for experiments at 3 K, kinetic measurements for the rearrangement of **3c** at 10 and 18 K resulted in estimated rate constants (k_3) of ~6.0 × 10^{-5} s^{-1} ($t_{1/2}$ ~195 min) and ~7.0 × 10^{-5} s^{-1} ($t_{1/2}$ ~165 min), respectively
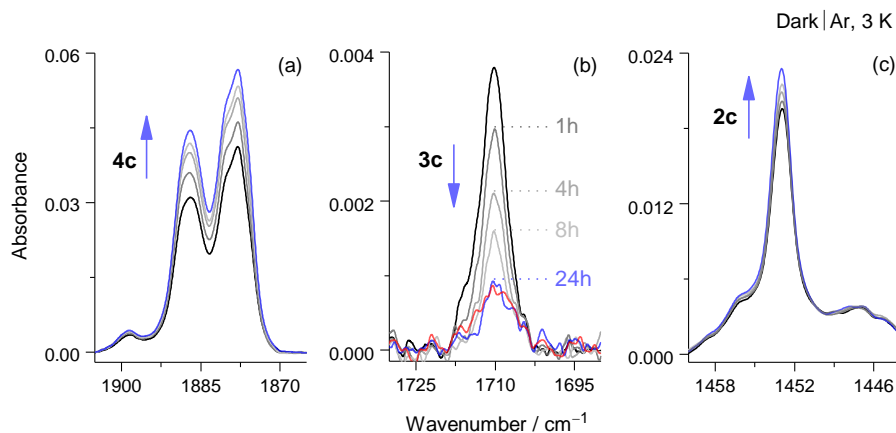
Figure 4. Time evolution of infrared spectra showing the disappearance of benzazirine **3c** and the simultaneous growth of both ketenimine **4c** and triplet nitrene **2c** *via* quantum mechanical tunneling in an argon matrix at 3 K. During the measurements, a cutoff filter transmitting below 2200 cm^{-1} was placed between the spectrometer light source and the sample. Between the measurements, the sample was protected from the spectrometer light source by a black plate. The black line represents $t = 0$, the solid grey lines at different shades represent $t = 1$, 4, and 8 h, and blue line represents $t = 24$ h (for more details see also Figure S6). The spontaneous rearrangement of **3c** is essentially completed after 24 h as shown (panel b) by comparing the spectrum after 24 h decay (blue) with the spectrum before production of **3c** (red).

(Figures S7–S10). Even considering the data from a semi-quantitative perspective, due the rough precision of the estimations, it is evident that the rate of rearrangement of **3c** barely shows an increase upon increasing the absolute

4

temperature by a factor up to five. Moreover, the **2c**:**4c** ratio resulting from the decay of **3c** essentially does not change with an increase of temperature (estimated 18:82 at 10 K and 17:83 at 18 K). Thus, these data indicate that the rearrangements of **3c**, as well as the formation of products ³A₂-**2c** and **4c**, are not due to thermally activated processes but in line with two independent QMT reactions: a competitive process of nitrogen *versus* carbon tunneling in **3c** to form ³A₂-**2c** and **4c**, respectively (Scheme 3).

Computations. To better understand the nature of the observed transformations, we computed the PES around **3c** (Figure 5). The mechanism for the formation of ³A₂-**2c** conceivably involves the ring opening of **3c** to ¹A₂-**2c** followed by fast intersystem crossing (ISC). Because ¹A₂-**2c** cannot be adequately described using a single-determinant wavefunction, the complete surface was first computed at the CASSCF(8,8)/6-311+G(2d,p) level of theory. To include dynamic electron correlation, single point energies were then computed at NEVPT2(8,8)/6-311+G(2d,p). With exceptions of ¹A₂-**2c** and **TS1**, all other stationary points were also computed at the CCSD(T)/cc-pVTZ//B3LYP/6-311+G(2d,p) level of theory (details are provided Experimental and Computational Methods section). The CASSCF and NEVPT2 approaches give a similar energy barrier for the ring-opening of **3c** to ¹A₂-**2c**, 2.8 and 2.5 kcal mol⁻¹, respectively.[43] Concerning the barrier for ring-expansion of **3c** to **4c**, NEVPT2 and CCSD(T) computations give substantially different values, namely 2.6 and 7.3 kcal mol⁻¹, respectively.[44] NEVPT2 computations most likely underestimate this energy barrier.[45] Previous CCSD(T) computations for the ring-expansion of a formyl derivative of benzazirine **3b** to the corresponding formyl substituted cyclic ketenimine **4b** provided a good rationalization for the experimental observations.[46] Thus, the barrier height for the ring-expansion of **3c** to **4c** is most probably close to 7 kcal mol⁻¹. Overall, computations show that the introduction of *para*-NH₂ substituent (EDG) considerably decreases the energy barrier for the ring-opening of **3c** to ¹A₂-**2c** and increases the energy barrier for the ring-expansion of **3c** to **4c**. Considering the process from **2c** to **4c**, the last step is rate-determining step (see also Figure S11).
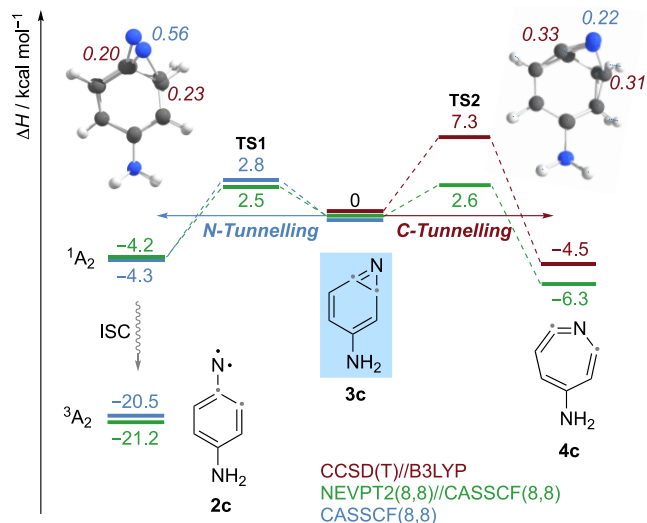

Figure 5. Reaction pathways of **3c** computed at CCSD(T)/cc-pVTZ//B3LYP/6-311+G(2d,p) + ZPVE (red), NEVPT(8,8)/6-311+G(2d,p)//CASSCF(8,8)6-311+G(2d,p) + ZPVE (green), and CASSCF(8,8)6-311+G(2d,p) + ZPVE (blue). ¹A₂ = open-shell singlet state, ³A₂ = triplet ground state, ISC = intersystem crossing, ZPVE = zero-point vibrational energy. Top left and right images show the structural overlap of the turning point geometries (color code: carbon: gray, nitrogen: blue, hydrogen: white) and the most significant tunneling distances of the individual atoms (arc lengths in Å in italics) involved in N- and C-tunneling, respectively (more details are given in Figures S14 and S15).

This is consistent with computations by Cramer et al.[39] concerning the PES of *para*-NHMe substituted phenylnitrene **2**. Even though the computed PES indicates that **3c** is separated from ¹A₂-**2c** by an energy barrier of only ~2.5 kcal mol⁻¹ (and from **4c** by a higher energy barrier), according to classic rate theory, **3c** should be stable at the cryogenic temperatures of the experiment, that is, it should *not* disappear over the course of the experiment. Based on the Arrhenius equation, the computed rate for over-the-barrier (thermal) transformation of **3c** to ¹A₂-**2c** gives a half-life time of ~10¹⁶² years at 3 K (see Experimental and Computational Methods section). An additional noteworthy feature is that the observed major product **4c**, resulting from the transformation of **3c**, actually is separated from the precursor by a *higher* computed energy barrier than the minor product ³A₂-**2c**. This contradicts the rules inferred from classical TST and cannot be explained in terms of a classical thermal over-the-barrier process, but only by considering the occurrence of heavy-atom QMT dominated by *tunneling control*.[23,26,47]

To test theoretically the possibility of heavy-atom tunneling in **3c**, we computed tunneling half-lives using the one-dimensional Wentzel-Kramers-Brillouin (WKB) formalism (see Experimental and Computational Methods section), which has proven to be sufficiently reliable for estimating light and heavy-atom tunneling rates for carbene rearrangements.[23,48–50] Based on the augmented NEVPT2//CASSCF computed reaction path from **3c** to ¹A₂-

2c, the computed half-life time of **3c** is ~6 min (Figure S12 and Table S6). Regarding the reaction path from **3c** to **4c**, based on augmented CCSD(T)//B3LYP data, the computed half-life time of **3c** is ~35 min (Figure S13 and Table S7).[46] Although the computed half-life time values are not expected to be completely accurate due to the complexity of this PES, they clearly reveal the existence of two competitive tunneling reactions from **3c**, in line with the experimental observations at cryogenic temperatures. Moreover, computations show that all atomic nuclei undergo displacements in both tunneling processes but with clear distinct contributions from a specific nucleus (Figures S14 and S15). For the ring-opening of **3c** to $^1A_2$-**2c**, the nitrogen atom in the three-membered ring is the heavy atom showing by far the largest displacement (a traversed arc of ~0.56 Å, Figures 5 and S14). Thus, this reaction must be considered a rare case of nitrogen atom tunneling. To the best of our knowledge, there is one theoretical paper indicating that N-tunneling may be at work in so-called "click reactions"[51] and there is only one experimental report mentioned the involvement of the nitrogen atom movement in a tunneling process.[21] Regarding the ring-expansion of **3c** to **4c**, the two carbon atoms in the three-membered ring are clearly the heavy atoms with the largest displacements (with a traversed arc of ~0.32 Å each, Figures 5 and S15), making this a case of carbon atom tunneling.

CONCLUSIONS

Experimentally deciphering the role of heavy-atom QMT is very challenging and its manifestations in chemistry are just being unraveled. The very few observations of heavy-atom QMT have opened the door for a new and deeper understanding of how to control chemical reactivity. We have shown here a new reactivity paradigm in this area, by demonstrating that a single, well-defined chemical starting material may react through two different potential energy barriers giving rise to two different products. This was made possible only through competitive carbon vs. nitrogen QMT, a process that could not have been predicted or rationalized by classical TST with its paradigm of kinetic vs. thermodynamic control only. Model systems as the one presented here for the first time provide hitherto unexplored and exciting opportunities for future research, for instance, how to selectively tune the tunneling probabilities to arrive exclusively at the N- or C-tunneling product. This new way of controlling chemical selectivity then finally takes the quantum nature of atoms and molecules fully into account.

EXPERIMENTAL AND COMPUTATIONAL METHODS

Sample: *p*-Azidoaniline **1c**: *p*-Azidoaniline hydrochloride (purchased from Aldrich; purity 97%) (100 mg) was neutralized in water (20 mL) with 1N NaOH (20 mL) and then extracted with ethyl acetate (3 × 20 mL). The organic phase was washed with brine and then dried with Na₂SO₄. Evaporation of the solvent (room temperature) gave the free base **1c** as a pale yellowish solid.[52] The sample was kept under vacuum, protected from light and stored in the freezer. Under these conditions, no decomposition was observed during months after the sample had been prepared.

Matrix Isolation Spectroscopy: In order to prepare low-temperature argon matrices a sample of solid **1c** was placed into a glass tube connected to the vacuum chamber of a helium-cooled cryostat (Sumitomo RDK 408D2 closed-cycle refrigerator with F-70 compressor unit) equipped with polished potassium bromide (KBr) outer windows. Prior to deposition of the matrices, **1c** was purified from the volatile impurities by pumping through the cryostat at room temperature. During deposition of the matrices, the sample tube was kept at room temperature (immersed in water bath at 20 °C) and vapors of **1c** were deposited together with a large excess of argon onto a polished cesium iodide (CsI) window (kept at 12 K) used as optical substrate. After the deposition, all samples were cooled or warmed to the temperature selected for carrying the experiment (at 3, 10 or 18 K), and were kept at this temperature both during irradiation and the monitoring of decays. The temperature was measured directly at the sample holder, by a silicon diode sensor connected to a digital controller Lake Shore 336.

The IR spectra, in the 400–4000 cm⁻¹ range and with resolution of 0.7 cm⁻¹, were recorded using a Bruker Vertex 70 FT-IR spectrometer, equipped with a deuterated L-alanine doped triglycine sulphate (DLaTGS) detector and a KBr beam splitter. For a single measurement, a total of 50 scans was accumulated. To avoid interference from atmospheric H₂O and CO₂, a stream of N₂ was continuously purged through the optical path of the spectrometer. In some experiments, the mid-IR spectra were recorded only in the 400–2200 cm⁻¹ range, with a standard Edmund Optics long-pass filter placed between the spectrometer sources and the cryogenic matrix windows.

UV/Vis Irradiation Experiments: The samples were irradiated (through the outer KBr or BaF₂ window of the cryostat) using a high-pressure mercury lamp (HBO 200, OSRAM) and a monochromator (Bausch & Lomb) with a bandwidth of 10 nm centered at the specified wavelength. In preliminary experiments, the samples were also irradiated (through the outer KBr window of the cryostat) using tunable narrowband (~0.2 cm⁻¹ spectral width) light provided by a Spectra Physics Quanta-Ray MOPO-SL optical parametric oscillator (OPO) pumped with a pulsed Nd:YAG laser (repetition rate = 10 Hz, duration = 10 ns). For irradiations in the UV range (230–440 nm) the frequency-doubled beam (signal or idler) was used (pulse energy ~ 1 mJ) and for irradiations in the visible range (440–550 nm) the signal beam was used (pulse energy ~ 10 mJ). The outcome of UV/Vis irradiations (consumption of the reactant and generation of photoproducts) was monitored by collecting IR spectra of the irradiated samples.

Kinetics: During the decay of **3c** into $^3A_2$-**2c** and **4c** the sample was kept in the dark with the only exception when

6

monitoring IR spectra, which was performed using a cutoff filter transmitting only below 2200 cm^{-1} (placed between the sample and the spectrometer IR globar source). Moreover, to minimize the exposure of the sample to IR radiation, only a few spectra were collected during a period of several hours. A spectrum was collected at $t = 0.5$ h and then in steps of 1 h until reaching $t = 8$ h. A final spectrum was registered at $t = 24$ h. Each of these spectra was collected using 50 scans. Under such conditions, the collection length of one spectrum equals to 225 seconds. In the kinetic analysis, the moment of registration of the first spectrum was assumed to be the origin of decay time ($t = 0$ h) and the intensity of the benzazirine **3c** bands present in this first spectrum was assumed to be 100%. The amount of **3c** was followed by the peak intensity of the most characteristic absorption band at 1710 cm^{-1}, which does not overlap significantly with bands of the reactant or of other products. The decays observed in the presented experiments were fitted, for a rough estimation of the rate constants, using the equation of a single-exponential decay:

$$[R]_t = [R]_0 \exp[-k_3 t].$$

Here, we observe a competing first-order reaction of a single reactant to give two different products. The overall rate of disappearance of **3c** (k_3) is the sum of the rates of the two routes leading to products $^3A_2$-**2c** (k_2) and **4c** (k_4), respectively: $k_3 = k_2 + k_4$. Therefore, to evaluate k_2 and k_4 separately, we determined the ratio of the products formed: $k_2/k_4 = [^3A_2$-**2c**]/[**4c**]. Since during irradiation at 350 nm ketenimine **4c** is selectively converted to triplet nitrene $^3A_2$-**2c**, the corresponding IR spectra were used to obtain a normalization factor. By applying this normalization factor to the corresponding difference IR spectra obtained as results of the decay of **3c**, the $^3A_2$-**2c**:**4c** branching ratio was obtained. This procedure was done by considering the area of the most characteristic absorption band of $^3A_2$-**2c** at 1453 cm^{-1} and of **4c** at 1887/1878 cm^{-1}. Then, using this estimated branching ratio and the decay rate of **3c** (k_3) the rates of formation of $^3A_2$-**2c** (k_2) and **4c** (k_4) were estimated.

IR Spectra Computations: For the purpose of interpretation of the experimental IR spectra, geometry optimizations and harmonic frequency computations were performed at the B3LYP/6-311+G(2d,p) level of theory, using Gaussian 09 (Revision D.01).[53] To assure accuracy of the results, all computations were performed using tight optimization criteria, an ultrafine integration grid and an enhancement of the threshold for integral accuracy by two orders of magnitude, comparing to the default threshold (10^{-12} rather than 10^{-10}), as recommended elsewhere.[54] Indeed, the last two options are now default in the next Gaussian 16 version.[55] The nature of stationary points was confirmed by the analysis of the Hessian matrices. In order to correct for the neglected anharmonic effects, incomplete treatment of electron correlation, and basis set limitations, the harmonic vibrational frequencies were scaled down. The scaling factors were obtained by fitting the computed frequencies of p-azidoaniline **1c** to the experimental frequencies of **1c**

(see Figure S1 and Table S1), separately in two frequency regions. In the 400–1700 cm^{-1} range, 23 experimental and computed frequencies were used to carry out a least-squares linear fit, with intercept zero ($y = bx$). The correlation coefficient was $R^2 = 0.99997$, and the obtained slope $b = 0.979$ (see Figure S2). This value of 0.979 was used across this study as the scaling factor for the computed harmonic frequencies in the 400–3000 cm^{-1} range, both for the reactant and for the photoproducts. In the higher frequency range, fitting of the two NH stretching modes [$\nu_{as}(NH_2)$ and $\nu_s(NH_2)$] resulted in the scaling factor equal to 0.960. This factor was then used to scale down computed frequencies in the range above 3000 cm^{-1}.

After scaling the computed frequencies by factors of 0.979 and 0.960 (below and above 3000 cm^{-1}, respectively), the resulting frequencies, together with the computed infrared intensities, were convoluted with Lorentzian functions having a full width at half-maximum (FWHM) of 2 cm^{-1}. In the simulated spectra, the peak intensities of the convoluted bands were set equal to the computed IR intensities (in km mol^{-1}); the simulations were carried out using the ChemCraft software.[56]

It is well-known that the out-of-plane vibrations of the NH$_2$ group in primary amines are strongly anharmonic and are difficult to describe computationally.[57–60] This is also true for p-azidoaniline **1c**, which exhibits strongly anharmonic vibration due to the $\omega(NH_2)$ mode (see Figure S1, part 4), with a very intense infrared band. Its computed (scaled) frequency is 586 cm^{-1}, and it was assigned to the experimental band at 429 cm^{-1}, the only intense infrared band computed and observed below 600 cm^{-1} (see Figure S1, part 4). Taking into account the strong anharmonicity of the $\omega(NH_2)$ mode, it was not used in the least-squares linear fitting (see Figure S2). For the same reason, the spectral range below 600 cm^{-1} was not implemented in the process of the vibrational assignments of the generated photoproducts $^3A_2$-**2c**, **3c**, and **4c**. The study of the anharmonicity of the $\omega(NH_2)$ mode is beyond the scope of the present study.

The NH$_2$ group in the studied compounds is non-planar, and may give rise to two conformers. These two conformers always co-exist and are connected by inversion of the amino-group (the $\omega(NH_2)$ mode), which has a strong tunneling contribution.[57–60] For p-azidoaniline **1c** and triplet p-aminophenylnitrene $^3A_2$-**2c** the amino group is connected to a planar aromatic ring, and the two conformers resulting from the inversion of the amino group are identical by symmetry. However, the amino-substituted benzazirine **3c** and the amino-substituted ketenimine **4c** possess non-planar heavy-atom backbones, and the inversion of the amino group formally produces two non-identical minima (for both **3c** and **4c**). We call these two minima "*syn*" and "*anti*", according to the relative orientations of the amino group hydrogen atoms, with respect to the nitrogen atom on the opposite end of the molecule (azirine nitrogen atom for **3c**, or ketenimine nitrogen atom for **4c**). The geometries of *syn*- and *anti*- minima were optimized, and respective

7

vibrational spectra were computed. They are shown graphically in Figure S16 (*anti*-**3c** and *syn*-**3c**), and in Figure S17 (*anti*-**4c** and *syn*-**4c**). These computed spectra are also collected in Table S8 and Table S9. Each pair of conformers has very similar vibrational signatures, including the predicted frequencies of characteristic stand-alone bands used for kinetic measurements: v(C=N) mode for **3c** (shown in bold in Table S8), and the v_{as}(C=C=N) mode for **4c** (shown in bold in Table S9). In the 700–2000 cm⁻¹ spectral range used for vibrational assignments, the mean absolute difference in predicted (unscaled) vibrational frequencies is below 2 cm⁻¹ for **3c** (*syn*-**3c** minus *anti*-**3c**), and below 4 cm⁻¹ for **4c** (*syn*-**4c** minus *anti*-**4c**).

The thermochemistry was also analyzed. In both pairs, the *syn*- forms are marginally more stable than *anti*-forms: by 0.26 kcal mol⁻¹ for **3c**, and by 0.56 kcal mol⁻¹ for **4c** (these zero-point vibrational energy corrected energies were computed at the B3LYP/6-311+G(2d,p) level). As mentioned above, the inversion of the amino-group is tunneling-assisted and the *syn*- and *anti*- conformers do not exist individually, either for **3c** or for **4c**. For the sake of further analysis, the *syn*- forms of **3c** and **4c** were used throughout this work.

Computations of PES: For the purpose of analyzing the PES around **3c**, the complete surface was first computed at CASSCF(8,8)/6-311+G(2d,p) level of theory using Gaussian 16 program package.[61] An eight-electron, eight-orbital active space (8,8) was used for all species, as described previously for the PES around parent species **3a**.[33] For species **2c**, the active space consists of seven π and π^* molecular orbitals (MOs), plus the in-plane p atomic orbitals (AO) on nitrogen. For species **3c**, the active space involves six π and π^* MOs, plus a σ/σ^* pair for the ring C–N bond. For species **4c**, the four π and the four π^* MOs of the double bonds were used. For the two transition states, **TS1** and **TS2**, the active space consists of six orbitals of π character plus a σ/σ^* pair for the partially formed/broken bond. This active space has typically been used to compute the reaction paths from arylnitrenes **2** to cyclic ketenimines **4**,[35] and the justification for its choice is addressed in ref. 33. After geometry optimizations, the harmonic vibrational frequencies were computed at the same level of theory. The nature of stationary points was confirmed by the analysis of the corresponding Hessian matrices. The CASSCF(8,8)/6-311+G(2d,p) vibrational frequencies were also used to compute the zero-point vibrational corrections to the energies. To include dynamic electron correlation, single point energies were then computed at NEVPT2(8,8)/6-311+G(2d,p) at the CASSCF(8,8)/6-311+G(2d,p) optimized geometries. With exceptions of ¹A₂-**2c** and **TS1**, all the other stationary points were also computed at the CCSD(T)/cc-pVTZ at the B3LYP/6-311+G(2d,p) optimized geometries. Note that the T_1 diagnostic ($T_1 = 0.028$) indicates that **TS1** cannot be computed adequately at the CCSD(T) level of theory (or using another single-determinant wavefunction method).[62] All NEVPT2 and CCSD(T) computations were performed with the ORCA program package and the default program settings.[63]

Computation of the Over-the-Barrier Reaction Rate of 3c: The Arrhenius equation applied to the reaction of **3c** to ¹A₂-**2c** gives a rate of ~2 × 10⁻¹⁷⁰ s⁻¹ and a half-life time of about 10¹⁶² years at 3 K, based on the computed energy barrier of 2.5 kcal mol⁻¹ and assuming a pre-exponential factor A = 2.8 × 10¹² s⁻¹, estimated from literature for a similar reaction (ring-opening of a fluoro-derivative benzazirine **3** to the corresponding nitrene ¹A₂-**2**).[40] Note that the intersystem crossing (ISC) from ¹A₂-**2c** to ³A₂-**2c** is an extremely fast process (experimentally determined value for parent phenylnitrene **2a** is k_{ISC} ~3.8 × 10⁶ s⁻¹; $t_{1/2}$ ~1 ns),[64] and for this reason the rates estimated for reaction of **3c** to ¹A₂-**2c** are assumed to be essentially the same as for the transformation of **3c** to ³A₂-**2c**.

Tunneling Computations: For the estimation of the tunneling rate, we mapped out the intrinsic reaction coordinates (IRC) starting from **TS1** and **TS2** at CASSCF(8,8)/6-311+G(2d,p) and B3LYP/6-311+G(2d,p) level of theory, respectively. In order to do so, we employed the Hessian-based predictor-corrector integrator in a default mass–weighted coordinate system as implemented in Gaussian 16 electronic structure package.[61] Every point along the reaction part was augmented with higher level NEVPT2 and CCSD(T) single point energies, respectively. Zero-point vibrational energy corrections for all modes orthogonal to the reaction path were added to the overall reaction profiles at NEVPT2//CASSCF+ZPVE and CCSD(T)//B3LYP+ZPVE level of theory. The corrected potential along the reaction coordinate ξ was then characterized by interpolating function V(ξ). The attempt frequency of barrier penetration, ω_o, was identified by comparing the starting material's frequencies and the projected frequencies along the IRC. The barrier penetration integral σ between the classical turning points s_1 and s_2, where V(ξ) = ε was computed as:

$$\sigma = \frac{1}{\hbar} \int_{s_1}^{s_2} \sqrt{2(V(\xi) - \xi)} \, d\xi$$

Tunneling probabilities κ_{WKB} were calculated by numerically integrating the barrier penetration integral σ and using the WKB equation.[65–69]

$$\kappa_{WKB} = \frac{1}{1 + e^{2\sigma}}$$

The corresponding tunneling half-life time τ was computed by employing a first order kinetic rate law:

$$\tau = \frac{\ln(2)}{\omega_0 \, \kappa_{WKB}}$$

The tunneling distances (arc lengths as the IRC coordinate are multidimensional) of every atom along the reaction path between the two turning points were obtained by summing up the atom distances between every specific point along the IRC. For the Euclidian

distances, only the atom distances of the two turning points geometries were determined.

ASSOCIATED CONTENT

AUTHOR INFORMATION

Corresponding Author

*cmnunes@qui.uc.pt
*prs@uni-giessen.de

Author Contributions

C.M.N. and A.K.E. performed the experiments and conducted all computations. C.M.N., A.K.E., I.R., and P.R.S. analyzed the data. C.M.N. conceived the original working hypothesis. All authors co-wrote the manuscript.

Notes
The authors declare no competing interests.

ACKNOWLEDGMENT

REFERENCES

(1) *Atom Tunneling Phenomena in Physics, Chemistry and Biology*; Miyazaki, T., Ed.; Springer-Verlag, Berlin, 2004.

(2) Sheridan, R. S. Quantum Mechanical Tunneling in Organic Reactive Intermediates. In *Reviews of Reactive Intermediate Chemistry*; Moss, R. A., Platz, M. S., Jones, M. J., Eds.; John Wiley & Sons, 2006; pp 415–463.

(3) Bell, R. P. *The Tunnel Effect in Chemistry*; Springer, US, Boston

(4) Greer, E. M.; Kwon, K.; Greer, A.; Doubleday, C. Thermally Activated Tunneling in Organic Reactions. *Tetrahedron* 2016, 72, 7357–7373.

(5) Layfield, J. P.; Hammes-Schiffer, S. Hydrogen Tunneling in Enzymes and Biomimetic Models. *Chem. Rev.* 2014, 114, 3466–3494.

(6) Shannon, R. J.; Blitz, M. A.; Goddard, A.; Heard, D. E. Accelerated Chemistry in the Reaction between the Hydroxyl Radical and Methanol at Interstellar Temperatures Facilitated by Tunnelling. *Nat. Chem.* 2013, 5, 745–749.

(7) Ley, D.; Gerbig, D.; Schreiner, P. R. Tunnelling Control of Chemical Reactions - the Organic Chemist's Perspective. *Org. Biomol. Chem.* 2012, 10, 3781–3790.

(8) Nagel, Z. D.; Klinman, J. P. Update 1 of: Tunneling and Dynamics in Enzymatic Hydride Transfer. *Chem. Rev.* 2010, 110, PR41–PR67.

(9) Schreiner, P. R.; Reisenauer, H. P.; Pickard, F. C.; Simmonett, A. C.; Allen, W. D.; Mátyus, E.; Császár, A. G.

Capture of Hydroxymethylene and Its Fast Disappearance through Tunnelling. *Nature* 2008, 453, 906–909.

(10) Nagel, Z. D.; Klinman, J. P. Tunneling and Dynamics in Enzymatic Hydride Transfer. *Chem. Rev.* 2006, 106, 3095–3118.

(11) Truhlar, D. G. Tunneling in Enzymatic and Nonenzymatic Hydrogen Transfer Reactions. *J. Phys. Org. Chem.* 2010, 23, 660–676.

(12) Borden, W. T. Reactions That Involve Tunneling by Carbon and the Role That Calculations Have Played in Their Study. *WIREs Comput. Mol. Sci.* 2015, 6, 20–46.

(13) Orendt, A. M.; Arnold, B. R.; Radziszewski, J. G.; Facelli, J. C.; Malsch, K. D.; Strub, H.; Grant, D. M.; Michl, J. ^{13}C NMR and Polarized IR Spectra of Vicinally Labeled [$^{13}C_2$]Cyclobutadiene in an Argon Matrix: Interconversion of Valence Tautomers. *J. Am. Chem. Soc.* 1988, 110, 2648–2650.

(14) Zuev, P.; Sheridan, R. Tunneling in the C-H Insertion of a Singlet Carbene: *tert*-Butylchlorocarbene. *J. Am. Chem. Soc.* 1994, 116, 4123–4124.

(15) Zuev, P. S.; Sheridan, R. S.; Albu, T. V; Truhlar, D. G.; Hrovat, D. a; Borden, W. T. Carbon Tunneling from a Single Quantum State. *Science* 2003, 299, 867–870.

(16) Moss, R. A.; Sauers, R. R.; Sheridan, R. S.; Tian, J.; Zuev, P. S. Carbon Tunneling in the Ring Expansion of Noradamantylchlorocarbene. *J. Am. Chem. Soc.* 2004, 126, 10196–10197.

(17) Inui, H.; Sawada, K.; Oishi, S.; Ushida, K.; McMahon, R. J. Aryl Nitrene Rearrangements: Spectroscopic Observation of a Benzazirine and Its Ring Expansion to a Ketenimine by Heavy-Atom Tunneling. *J. Am. Chem. Soc.* 2013, 135, 10246–10249.

(18) Ertelt, M.; Hrovat, D. A; Borden, W. T.; Sander, W. Heavy-Atom Tunneling in the Ring Opening of a Strained Cyclopropene at Very Low Temperatures. *Chem. A Eur. J.* 2014, 20, 4713–4720.

(19) Nunes, C. M.; Reva, I.; Kozuch, S.; McMahon, R. J.; Fausto, R. Photochemistry of 2-Formylphenylnitrene: A Doorway to Heavy-Atom Tunneling of a Benzazirine to a Cyclic Ketenimine. *J. Am. Chem. Soc.* 2017, 139, 17649–17659.

(20) Schleif, T.; Mierez-Perez, J.; Henkel, S.; Ertelt, M.; Borden, W. T.; Sander, W. The Cope Rearrangement of 1,5-Dimethylsemibullvalene-2(4)-d$_1$: Experimental Evidence for Heavy Atom Tunneling. *Angew. Chem. Int. Ed.* 2017, 56, 10746–10749.

(21) Wu, Z.; Feng, R.; Li, H.; Xu, J.; Deng, G.; Abe, M.; Bégué, D.; Liu, K.; Zeng, X. Fast Heavy-Atom Tunneling in Trifluoroacetyl Nitrene. *Angew. Chem. Int. Ed.* 2017, 56, 15672–15676.

(22) Garrett, B. C.; Truhlar, D. G.; Bowman, J. M.; Wagner, A. F.; Robie, D.; Arepalli, S.; Presser, N.; Gordon, R. J. Ab Initio Predictions and Experimental Confirmation of Large Tunneling Contributions to Rate Constants and Kinetic Isotope Effects for Hydrogen Atom Transfer Reactions. *J. Am. Chem. Soc.* 1986, 108, 3515–3516.

(23) Schreiner, P. R. Tunneling Control of Chemical Reactions: The Third Reactivity Paradigm. *J. Am. Chem. Soc.* 2017, 139, 15276–15283.

(24) Notable exceptions are some very low-energy conformational isomerizations that can occur thermally (over-the-barrier) even in cryogenic matrices. See, for instance: Fausto, R., Khriachtchev, L., Hamm, P. "Conformational Changes in Cryogenic Matrices". In *Physics and Chemistry at Low Temperatures*; Khriachtchev, L., Ed.; Pan Stanford Publishing, 2012; pp 51–84.

(25) Doubleday, C.; Armas, R.; Walker, D.; Cosgriff, C. V.; Greer, E. M. Heavy-Atom Tunneling Calculations in Thirteen Organic Reactions: Tunneling Contributions Are Substantial, and Bell's Formula Closely Approximates Multidimensional Tunneling at ≥250 K. *Angew. Chem. Int. Ed.* 2017, 56, 13099–13102.

(26) Schreiner, P. R.; Reisenauer, H. P.; Ley, D.; Gerbig, D.; Wu, C.-H.; Allen, W. D. Methylhydroxycarbene: Tunneling Control of a Chemical Reaction. *Science* **2011**, *332*, 1300–1303.

(27) Gerbig, D.; Schreiner, P. R. Formation of a Tunneling Product in the Photo-Rearrangement of o-Nitrobenzaldehyde. *Angew. Chem. Int. Ed.* **2017**, *56*, 9445–9448.

(28) Mardyukov, A.; Quanz, H.; Schreiner, P. R. Conformer-Specific Hydrogen Atom Tunnelling in Trifluoromethylhydroxycarbene. *Nat. Chem.* **2017**, *9*, 71–76.

(29) Eckhardt, A. K.; Erb, F. R.; Schreiner, P. R. Conformer-Specific [1,2]*H*-Tunnelling in Captodatively-Stabilized Cyanohydroxycarbene (NC–Č–OH). *Chem. Sci.* **2019**, *10*, 802–808.

(30) *Nitrenes and Nitrenium Ions; Falvey, D. E.; Gudmundsdóttir, A. D., Eds.; John Wiley & Sons, 2013.*

(31) Platz, M. S. Nitrenes. In *Reactive Intermediate Chemistry*; Moss, R. A.; Platz, M. S.; Jones, M. J., Eds.; John Wiley & Sons, 2004; pp 501–559

(32) Wentrup, C. Carbenes and Nitrenes: Recent Developments in Fundamental Chemistry. *Angew. Chem. Int. Ed.* **2018**, *57*, 11508–11521

(33) Karney, W.; Borden, W. Ab Initio Study of the Ring Expansion of Phenylnitrene and Comparison with the Ring Expansion of Phenylcarbene. *J. Am. Chem. Soc.* **1997**, *119*, 1378–1387.

(34) Nunes, C. M.; Knezz, S. N.; Reva, I.; Fausto, R.; McMahon, R. J. Evidence of a Nitrene Tunneling Reaction: Spontaneous Rearrangement of 2-Formylphenylnitrene to an Imino Ketene in Low-Temperature Matrixes. *J. Am. Chem. Soc.* **2016**, *138*, 15287–15290.

(35) Gritsan, N. P.; Platz, M. S. Kinetics, Spectroscopy, and Computational Chemistry of Arylnitrenes. *Chem. Rev.* **2006**, *106*, 3844–3867.

(36) Grote, D.; Sander, W. Photochemistry of Fluorinated 4-Iodophenylnitrenes: Matrix Isolation and Spectroscopic Characterization of Phenylnitrene-4-Yls. *J. Org. Chem.* **2009**, *74*, 7370–7382.

(37) Morawietz, J.; Sander, W. Photochemistry of Fluorinated Phenyl Nitrenes: Matrix Isolation of Fluorinated Azirines. *J. Org. Chem.* **1996**, *61*, 4351–4354.

(38) Kozuch has nicely demonstrated that tunneling can be an additional factor to be taken into account in order to properly analyze the stability of a molecule. See for instance: Kozuch, S. A quantum mechanical "Jack in the box": Rapid Rearrangement of a Tetrahedryl-tetrahedrane via Heavy Atom Tunneling. *Org. Lett.* **2014**, *16*, 4102–4105.

(39) Johnson, W.; Sullivan, M. B.; Cramer, C. J. *meta* and *para* Substitution Effects on the Electronic State Energies and Ring-Expansion Reactivities of Phenylnitrenes. *Int. J. Quantum Chem.* **2001**, *85*, 492–508.

(40) To the best of our knowledge only in one more case (on the o-fluorophenylnitrene PES) it has been estimated that benzazirine **3** ring-opening to nitrene **2** would have a lower barrier that benzazirine **3** ring-expansion to cyclic ketenimine **4**. See: Gritsan, N. P.; Gudmundsdóttir, A. D.; Tigelaar, D.; Zhu, Z.; Karney, W. L.; Hadad, C. M.; Platz, M. S. A Laser Flash Photolysis and Quantum Chemical Study of the Fluorinated Derivatives of Singlet Phenylnitrene. *J. Am. Chem. Soc.* **2001**, *23*, 1951–1962.

(41) Pritchina, E. A.; Gritsan, N. P.; Bally, T. Matrix Isolation and Computational Study of the Photochemistry of P-Azidoaniline. *Phys. Chem. Chem. Phys.* **2006**, *8*, 719–727.

(42) Dispersive character is commonly observed for kinetics of this kind of reactions in cryogenic matrices. See, for example refs. (14-20, 34).

(43) Our NEVPT2 computations for the ring-opening of the parent species (**3a** to $^1A_2$-**2a**) give an energy barrier of 5.3 kcal

mol^{-1} (Figure S11), in good agreement with results reported by Karney and Borden[31] (5.1 kcal mol^{-1}) and Cramer et al.[37] (5.5 kcal mol^{-1}) at the CASPT2 level of theory.

(44) CASSCF computations are not discussed because they are known to considerably overestimate the energy barriers of highly delocalized transition states (such as in the case of transformation of **3** to **4**) due to the lack of dynamic electron correlation.[31,33]

(45) In support of this interpretation, NEVPT2 computations for the ring-expansion of the parent species (**3a** to **4a**) give an energy barrier of 0.3 kcal mol^{-1} (Figure S11) whereas CASPT2 computations carried out by Karney and Borden,[31] and Cramer et al.[37] give an energy barrier of ~3.1 kcal mol^{-1}.

(46) The computed CCSD(T) energy barrier from **3c** to **4c** is very similar to the computed barrier for the ring-expansion of a formyl derivative benzazirine **3b** to the corresponding formyl-substituted cyclic ketenimine **4b** (~7.5 kcal mol^{-1}) in which heavy-atom tunneling was previously observed.[18] Therefore, the existence of heavy-atom tunneling from **3c** to **4c** could be envisaged, showing the reliability of the computed data at the CCSD(T) level of theory.

(47) A referee of this work pointed that in the theoretical study of the kinetics of the H + *trans*-N_2H_2 reactions, variational effects, rather than tunneling, can be responsible for a scenario where the chemical reaction proceeds mainly through a higher-energy path. See: Zheng, J.; Rocha, R. J.; Pelegrini, M.; Ferrão, L. F. A.; Carvalho, E. F. V.; Roberto-Neto, O.; Machado, F. B. C.; Truhlar, D. G. A Product Branching Ratio Controlled by Vibrational Adiabaticity and Variational Effects: Kinetics of the H + *Trans*-N_2H_2 Reactions. *J. Chem. Phys.* **2012**, *136*, 184310.

(48) Eckhardt, A. K.; Gerbig, D.; Schreiner, P. R. Heavy Atom Secondary Kinetic Isotope Effect on H-Tunneling. *J. Phys. Chem. A* **2018**, *122*, 1488–1495.

(49) Gerbig, D.; Ley, D.; Schreiner, P. R. Light- and Heavy-Atom Tunneling in Rearrangement Reactions of Cyclopropylcarbenes. *Org. Lett.* **2011**, *13*, 3526–3529.

(50) The WKB model is a simple approximation that does not include corner-cutting effects like small-curvature tunneling (SCT), and therefore the computed half-lives can sometimes be overestimated. See for instance: Allison T. C., Truhlar D. G. Testing the Accuracy of Practical Semiclassical Methods: Variational Transition State Theory with Optimized Multidimensional Tunneling. In *Modern Methods for Multidimensional Dynamics Computations in Chemistry*; Thompson D. L. Eds.; World Scientific, Singapore, 1998, pp. 618-712.

(51) Karmakar, S.; Datta, A. Metal Free Azide-Alkyne Click Reaction: Role of Substituents and Heavy Atom Tunneling. *J. Phys. Chem. B* **2015**, *119*, 11540–11547.

(52) Lau, A. N. K.; Eason, R. G. *Polymers Having Orthogonal Reactive Groups and Uses Thereof.* Int. Patent WO/2014/059352, April 17, 2014.

(53) Frisch, M. J.; Trucks, G. W.; Schlegel, H. B.; Scuseria, G. E.; Robb, M. A.; Cheeseman, J. R.; Scalmani, G.; Barone, V.; Mennucci, B.; Petersson, G. A.; Nakatsuji, H.; Caricato, M.; Li, X.; Hratchian, H. P.; Izmaylov, A. F.; Bloino, J.; Zheng, G.; Sonnenberg, J. L.; Hada, M.; Ehara, M.; Toyota, K.; Fukuda, R.; Hasegawa, J.; Ishida, M.; Nakajima, T.; Honda, Y.; Kitao, O.; Nakai, H.; Vreven, T.; Montgomery, J. A., Jr.; Peralta, J. E.; Ogliaro, F.; Bearpark, M.; Heyd, J. J.; Brothers, E.; Kudin, K. N.; Staroverov, V. N.; Keith, T.; Kobayashi, R.; Normand, J.; Raghavachari, K.; Rendell, A.; Burant, J. C.; Iyengar, S. S.; Tomasi, J.; Cossi, M.; Rega, N.; Millam, J. M.; Klene, M.; Knox, J. E.; Cross, J. B.; Bakken, V.; Adamo, C.; Jaramillo, J.; Gomperts, R.; Stratmann, R. E.; Yazyev, O.; Austin, A. J.; Cammi, R.; Pomelli, C.; Ochterski, J. W.; Martin, R. L.; Morokuma, K.; Zakrzewski, V. G.; Voth, G. A.; Salvador, P.; Dannenberg, J. J.; Dapprich, S.;

Daniels, A. D.; Farkas, Ö.; Foresman, J. B.; Ortiz, J. V.; Cioslowski, J.; Fox, D. J. *Gaussian 09, Revision D.01*, Gaussian, Inc.: Wallingford CT, 2013.

(54) Foresman, J. B.; Frisch, A. *Exploring Chemistry with Electronic Structure Methods,* 3rd ed.; Gaussian, Inc.: Wallingford CT, 2015

(55) Changes from Gaussian 09 to Gaussian 16: http://gaussian.com/relnotes/ (last accessed April 26, 2019).

(56) Zhurko, G. A. *ChemCraft, Version 1.8*. http://www.chemcraftprog.com, 2016. (last accessed April 26, 2019).

(57) Howard, D. L.; Robinson, T. W.; Fraser, A. E.; Kjaergaard, H. G. The Effect of NH$_2$-Inversion Tunneling Splitting on the NH-Stretching Overtone Spectra of Aniline Vapour. *Phys. Chem. Chem. Phys.* **2004**, 719–724.

(58) Wojciechowski, P. M.; Zierkiewicz, W.; Michalska, D.; Hobza, P. Electronic Structures, Vibrational Spectra, and Revised Assignment of Aniline and Its Radical Cation: Theoretical Study. *J. Chem. Phys.* **2003**, *118*, 10900–10911.

(59) McCarthy, W. J.; Lapinski, L.; Nowak, M. J.; Adamowicz, L. Out-of-Plane Vibrations of NH$_2$ in 2-Aminopyrimidine and Formamide. *J. Chem. Phys.* **1998**, *108*, 10116–10128.

(60) McCarthy, W. J.; Lapinski, L.; Nowak, M. J.; Adamowicz, L. Anharmonic Contributions to the Inversion Vibration in 2-Aminopyrimidine. *J. Chem. Phys.* **1995**, *103*, 656–662.

(61) Frisch, M. J.; Trucks, G. W.; Schlegel, H. B.; Scuseria, G. E.; Robb, M. A.; Cheeseman, J. R.; Scalmani, G.; Barone, V.; Petersson, G. A.; Nakatsuji, H.; Li, X.; Caricato, M.; Marenich, A. V.; Bloino, J.; Janesko, B. G.; Gomperts, R.; Mennucci, B.; Hratchian, H. P.; Ortiz, J. V.; Izmaylov, A. F.; Sonnenberg, J. L.; Williams-Young, D.; Ding, F.; Lipparini, F.; Egidi, F.; Goings, J.; Peng, B.; Petrone, A.; Henderson, T.; Ranasinghe, D.; Zakrzewski, V. G.; Gao, J.; Rega, N.; Zheng, G.; Liang, W.; Hada, M.; Ehara, M.; Toyota, K.; Fukuda, R.; Hasegawa, J.; Ishida, M.; Nakajima, T.; Honda, Y.; Kitao, O.; Nakai, H.; Vreven, T.; Throssell, K.; Montgomery, J. A., Jr.; Peralta, J. E.; Ogliaro, F.; Bearpark, M. J.; Heyd, J. J.; Brothers, E. N.; Kudin, K. N.; Staroverov, V. N.; Keith, T. A.; Kobayashi, R.; Normand, J.; Raghavachari, K.; Rendell, A. P.; Burant, J. C.; Iyengar, S. S.; Tomasi, J.; Cossi, M.; Millam, J. M.; Klene, M.; Adamo, C.; Cammi, R.; Ochterski, J. W.; Martin, R. L.; Morokuma, K.; Farkas, O.; Foresman, J. B.; Fox, D. J. *Gaussian 16, Revision B.01*, Gaussian, Inc., Wallingford CT, 2016.

(62) Lee, T. J.; Taylor, P. R. A Diagnostic for Determining the Quality of Single-reference Electron Correlation Methods. *Int. J. Quantum Chem.* **1989**, *36*, 199–207.

(63) Neese, F. The ORCA Program System. *Wiley Interdiscip. Rev. Comput. Mol. Sci.* **2012**, *2*, 73–78.

(64) Gritsan, N. P.; Zhu, Z.; Hadad, C. M.; Platz, M. S. Laser Flash Photolysis and Computational Study of Singlet Phenylnitrene. *J. Am. Chem. Soc.* **1999**, *121*, 1202–1207.

(65) Kramers, H. A. Wellenmechanik und halbzahlige Quantisierung. *Zeitschrift für Phys.* **1926**, *39*, 828–840.

(66) Wentzel, G. Eine Verallgemeinerung der Quantenbedingungen für die Zwecke der Wellenmechanik. *Zeitschrift für Phys.* **1926**, *38*, 518–529.

(67) Brillouin, L. La Mécanique Ondulatoire de Schrödinger: Une Méthode Générale de Resolution par Approximations Successives. *C. R. Acad. Sci* **1926**, *183*, 24–26.

(68) Isaacson, A. D.; Truhlar, D. G. Polyatomic Canonical Variational Theory for Chemical Reaction Rates. Separable-Mode Formalism with Application to OH+H$_2$→H$_2$O+H. *J. Chem. Phys.* **1982**, *76*, 1380–1391.

(69) Garrett, B. C.; Truhlar, D. G. Semiclassical Tunneling Calculations. *J. Phys. Chem.* **1979**, *83*, 2921–2926.

Table of Contents

Competitive Tunneling

Nitrogen Tunneling · Carbon Tunneling
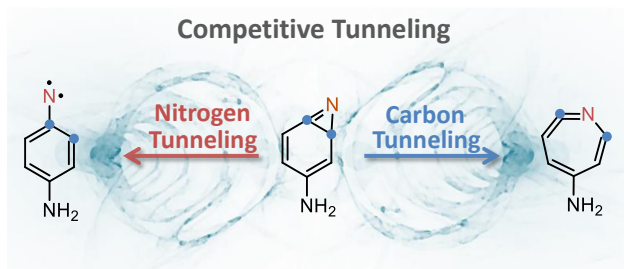
Supporting Information

Competitive nitrogen versus carbon tunneling

Cláudio M. Nunes,[1]* André K. Eckhardt,[2] Igor Reva,[1] Rui Fausto,[1] Peter R. Schreiner[2]*

[1]CQC, Department of Chemistry, University of Coimbra, 3004-535 Coimbra, Portugal

[2]Institute of Organic Chemistry, Justus Liebig University Giessen, Heinrich-Buff-Ring 17, 35392 Giessen, Germany

*e-mail: cmnunes@qui.uc.pt; prs@uni-giessen.de

Table of Contents

I. Additional Experimental Details

Note regarding UV-Vis spectra of ^{3}A$_2$-2c, 3c and 4c: It was observed that ketenimine **4c** was also selectively converted to ^{3}A$_2$-**2c** using narrowband irradiation at $\lambda = 500$ nm (or slightly shorter wavelengths) provided by a laser-OPO system. Although there are no well-defined absorptions in this region of the UV-Vis spectrum (Figure S3), this result suggests that **4c** has a very weak and broad band extending up to 500 nm. In the UV-Vis spectrum, a weak and broad absorption near 350 nm can be assigned to **4c**, which is consistent with TD-B3LYP/6-311+G(2d,p) computations that give the most intense electronic transition of **4c** at 351.8 nm ($f = 3.21 \times 10^{-2}$). For ^{3}A$_2$-**2c**, the UV-Vis spectrum shows structured bands in the 380−475 nm and 305−335 nm regions and a stronger band with maximum at ~283 nm, in agreement with results reported earlier (*ref. 39 in the main text*). The fact that **4c** absorbs in the visible region at longer wavelengths than ^{3}A$_2$-**2c** (as shown by the irradiation at 500 nm) also agrees reasonably well with TD-B3LYP/6-311+G(2d,p) computations, which give the lowest energy transition of **4c** at 398.2 nm ($f = 1.05 \times 10^{-2}$) and that of ^{3}A$_2$-**2c** at 396.7 nm ($f = 1.06 \times 10^{-2}$). No UV/Vis absorption bands could be assigned to amino-substituted benzazirine **3c** (Figure S5).

The electronic absorption spectra of ^{3}A$_2$-**2c**, **3c**, and **4c** were estimated using time dependent (TD) density functional theory (as implemented in the Gaussian 09 program package) at B3LPY/6-311+G(2d,p) level of theory. The computed excitation wavelengths (not scaled, listed only values with $\lambda > 250$ nm and with $f > 1 \times 10^{-4}$) are:

^{3}A$_2$-**2c**: 396.7 nm ($f = 1.05 \times 10^{-2}$), 384.4 nm ($f = 4.48 \times 10^{-2}$), 329.2 nm ($f = 2.74 \times 10^{-2}$), 312.4 nm ($f = 1.23 \times 10^{-2}$), 291.4 nm ($f = 3.3 \times 10^{-3}$), 290.5 nm ($f = 8.60 \times 10^{-2}$), 272.3 nm ($f = 3.8 \times 10^{-3}$), 260.9 nm ($f = 1.473 \times 10^{-1}$), 260.9 nm ($f = 2 \times 10^{-4}$), and 256.7 nm ($f = 4.88 \times 10^{-2}$);

3c: 376.3 nm ($f = 1.47 \times 10^{-2}$), 302.7 nm ($f = 4.39 \times 10^{-2}$), 270.9 nm ($f = 2.49 \times 10^{-2}$) and 258.8 nm ($f = 2.4 \times 10^{-3}$);

4c: 398.2 nm ($f = 1.06 \times 10^{-2}$), 351.8 nm ($f = 3.21 \times 10^{-2}$), 271.2 nm ($f = 3.1 \times 10^{-3}$), and 260.4 nm ($f = 6.8 \times 10^{-3}$).

II. Figures

Figure S1, part 1. (a) Experimental IR spectrum of *p*-azidoaniline **1c** isolated in an Ar matrix at 3 K. "w" designates bands due to monomeric water. Red squares designate combination bands [$\nu_{as}(NH_2) + \omega(NH_2)$, 3945 cm^{-1}] and [$\nu_{s}(NH_2) + \omega(NH_2)$, 3854 cm^{-1}). (b) IR spectrum of **1c** computed at the B3LYP/6-311+G(2d,p) level of theory. Computed wavenumbers were scaled by 0.960.
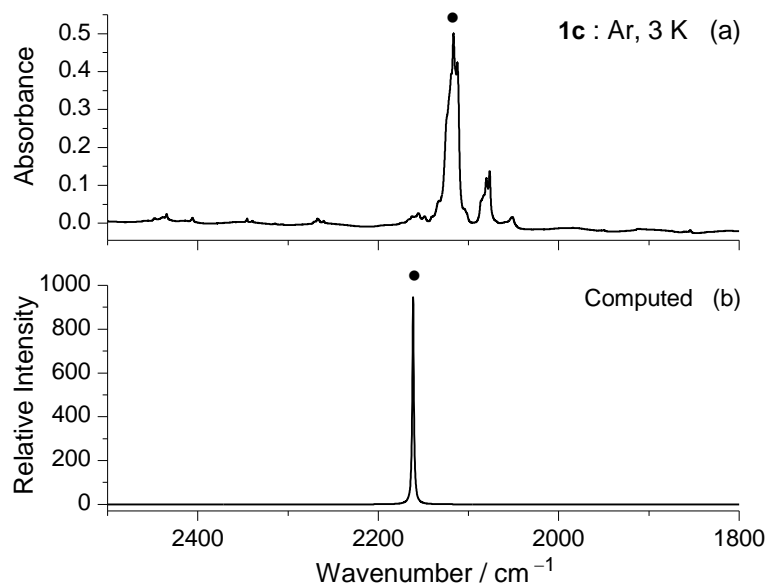
Figure S1, part 2. (a) Experimental IR spectrum of *p*-azidoaniline **1c** isolated in an Ar matrix at 3 K. (b) IR spectrum of **1c** computed at the B3LYP/6-311+G(2d,p) level of theory, showing the band due to the $\nu_{as}(N_3)$ vibration. The computed wavenumber was scaled by 0.979.
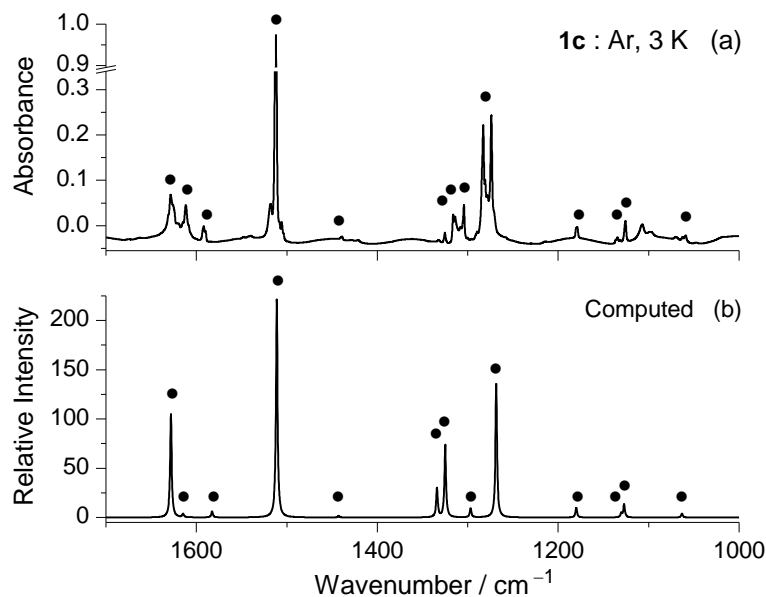
Figure S1, part 3. (a) Experimental IR spectrum of *p*-azidoaniline **1c** isolated in an Ar matrix at 3 K. Note the ordinate break. (b) IR spectrum of **1c** computed at the B3LYP/6-311+G(2d,p) level of theory. Computed wavenumbers were scaled by 0.979.

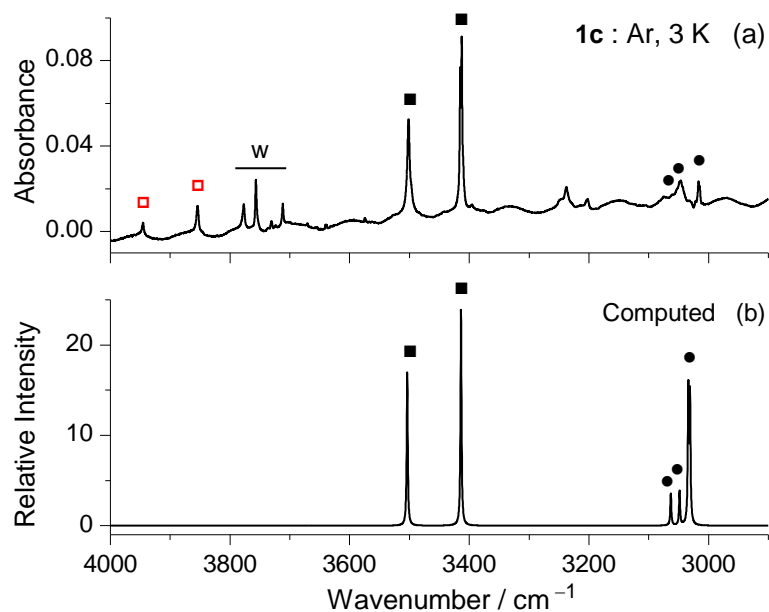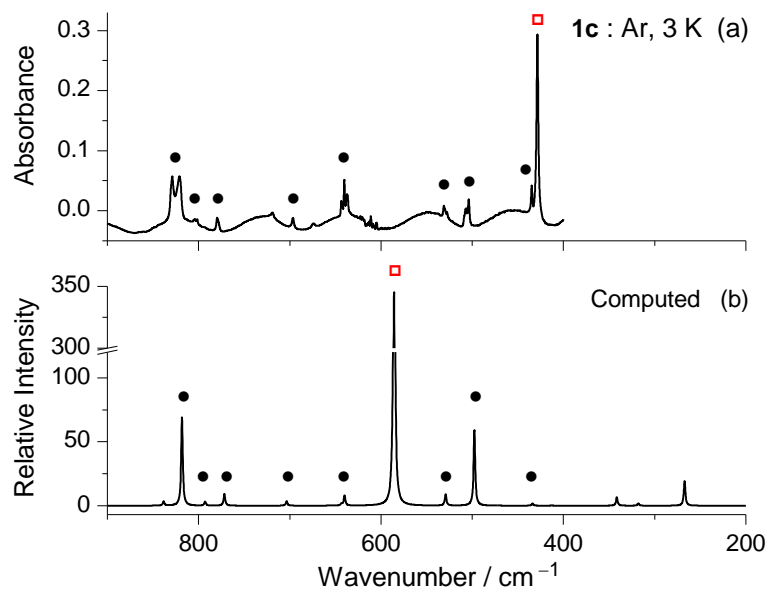**Figure S1, part 4.** (a) Experimental IR spectrum of *p*-azidoaniline **1c** isolated in an Ar matrix at 3 K. Red square designates the band assigned to the $\omega(NH_2)$ mode. (b) IR spectrum of **1c** computed at the B3LYP/6-311+G(2d,p) level of theory. Computed wavenumbers were scaled by 0.979. Red square designates the intense band due to the $\omega(NH_2)$ mode. Note the ordinate break.
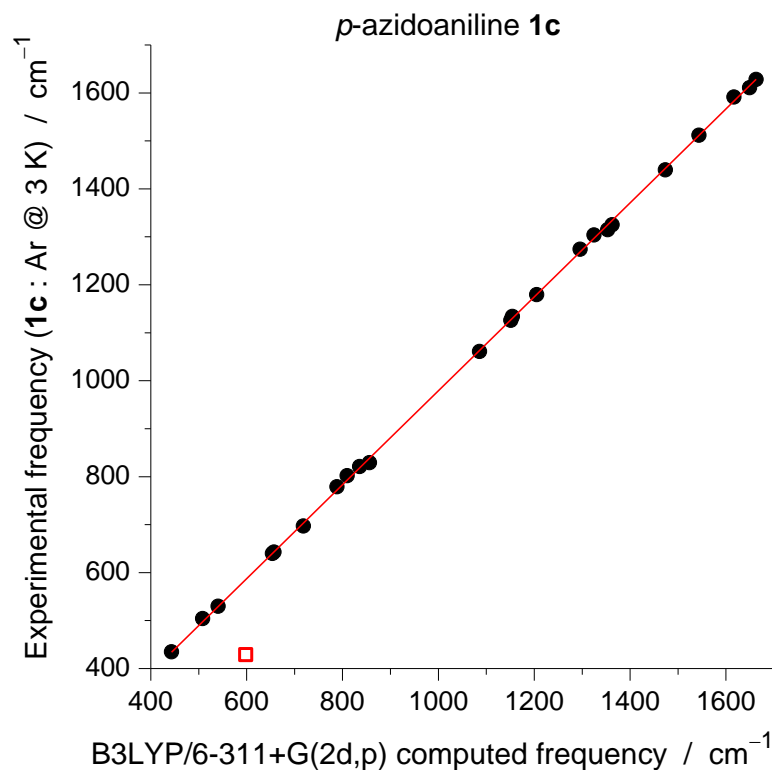
Figure S2. Circles: experimental frequencies observed in the IR spectrum of *p*-azidoaniline **1c** isolated in an argon matrix at 3 K compared to the B3LYP/6-311+G(2d,p) computed harmonic frequencies of **1c**. Red line: least-squares linear fit of 23 experimental and computed frequencies in the 400−1700 cm^{-1} range with intercept zero ($y = bx$). The correlation coefficient R^2 = 0.99997. The obtained slope b = 0.979, was used across this study as the scaling factor for the computed harmonic frequencies in the 400−3000 cm^{-1} range, both for the reactant and for the photoproducts. The red square shows strongly anharmonic intense infrared band due to the ω(NH$_2$) mode (see Figure S1, part 4), which was not used in the fitting procedure.
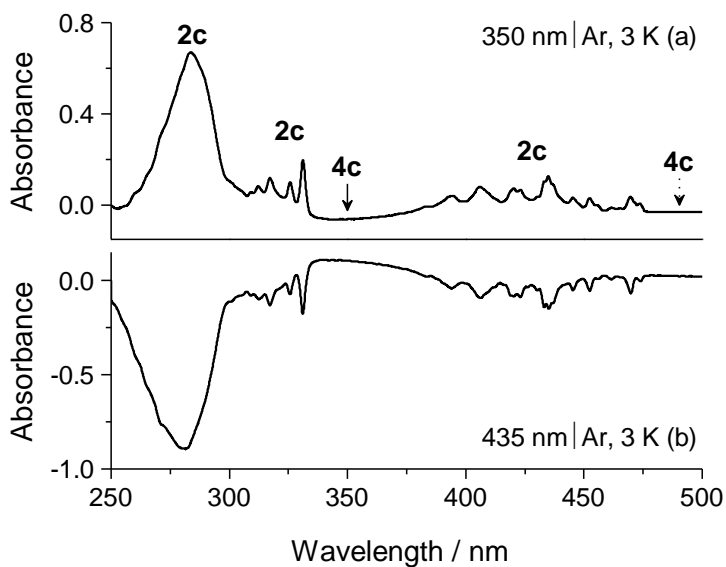
Figure S3. Difference UV/Vis spectra (sample in argon at 3 K) after (a) consumption of amino-substituted ketenimine **4c** with irradiation at $\lambda = 350$ nm, and (b) consumption of triplet *p*-aminophenylnitrene $^3A_2$-**2c** with irradiation at $\lambda = 435$ nm. UV/Vis absorption bands assigned to $^3A_2$-**2c** and **4c** are marked with the respective numbers.
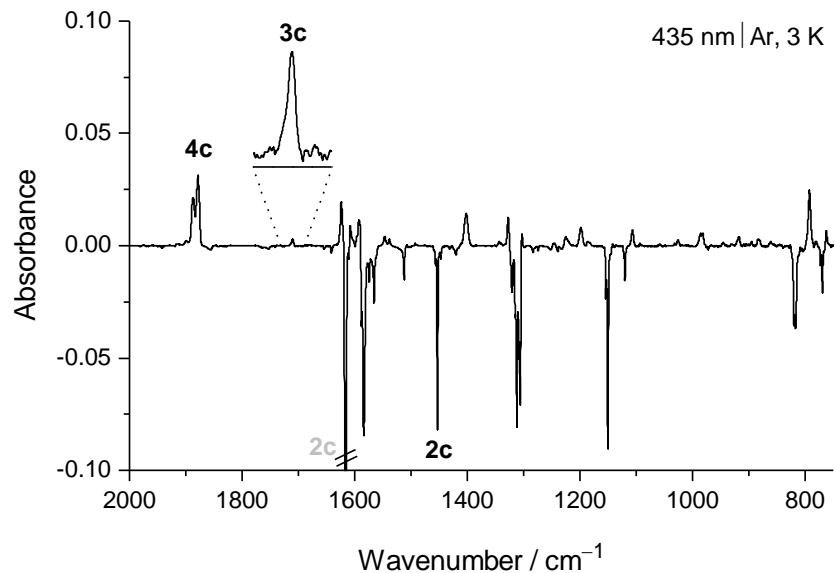
Figure S4. Experimental difference IR spectrum showing changes after irradiation at $\lambda = 435$ nm (8 min; argon matrix at 3 K), subsequent to irradiation at $\lambda = 350$ nm (Figure 2). The negative bands are due to the consumed triplet *p*-aminophenylnitrene $^3A_2$-**2c**. The positive bands are due to amino-substituted ketenimine **4c** and benzazirine **3c**. Similar results were obtained when irradiations were performed using other wavelengths within the range of 380–475 nm, corresponding to the absorption of a first structured band of $^3A_2$-**2c** (Figure S3). Irradiation at $\lambda = 435$ nm was selected because at this wavelength our high-pressure mercury lamp provides higher output power.
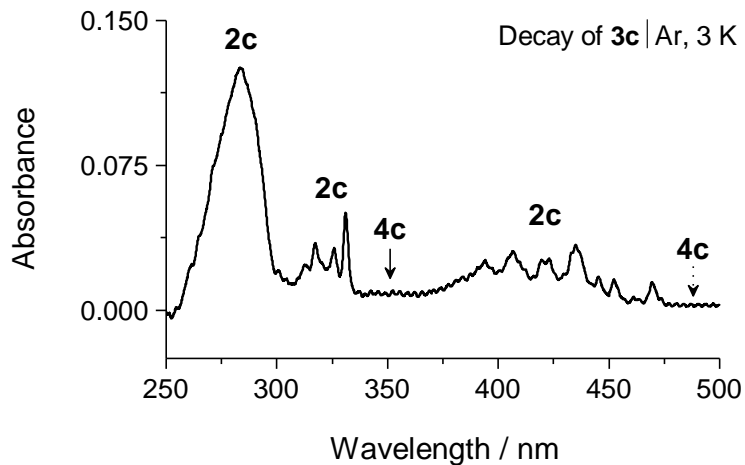
Figure S5. Difference UV/Vis spectrum (sample in argon at 3 K), growing after the decay of amino-substituted benzazirine **3c**. UV/Vis absorption bands assigned to $^3A_2$-**2c** and **4c** are marked with the respective numbers. No experimental UV-Vis absorptions could be assigned/detected for **3c**. This is probably because of the very small amount of **3c** produced and the possible overlap with UV-Vis bands of $^3A_2$-**2c** and **4c** (compare with Figure S3).

Figure S6. Kinetics of rearrangement of benzazirine **3c** to triplet nitrene $^3A_2$-**2c** and ketenimine **4c** in an argon matrix at 3 K under dark conditions. The spectra were recorded while protecting the sample with an infrared long-pass cutoff filter transmitting only below 2200 cm^{-1}. Black circles (●) represent the time evolution of the amount of **3c** (consumption, measured using the peak at 1710 cm^{-1}). The dotted line represents the best fit obtained using a first-order exponential decay kinetics equation. The rate constant obtained is $k_3 = 5.5 \times 10^{-5}$ s^{-1} corresponding to a half-life time of 210 min. The product rate constants are then estimated to be $k_2 \sim 8.3 \times 10^{-6}$ s^{-1} and $k_4 \sim 4.7 \times 10^{-5}$ s^{-1} (see the Experimental and Computational Methods section in the main text for more details).
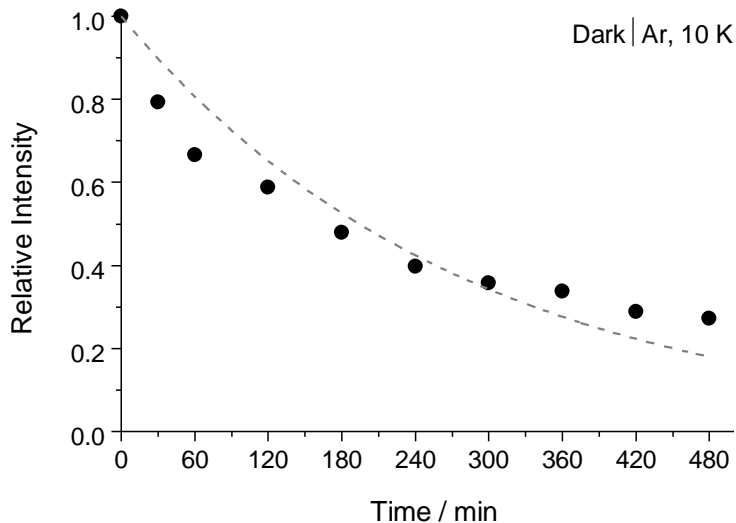
Figure S7. Kinetics of rearrangement of benzazirine **3c** to triplet nitrene $^3A_2$-**2c** and ketenimine **4c** in an argon matrix at 10 K under dark conditions. The spectra were recorded while protecting the sample with an infrared long-pass cutoff filter transmitting only below 2200 cm^{-1}. Black circles (●) represent the time evolution of the amount of **3c** (consumption, measured using the peak at 1710 cm^{-1}). The dotted line represents the best fit obtained using a first-order exponential decay kinetics equation. The rate constant obtained is $k_3 = 6.0 \times 10^{-5}$ s^{-1} corresponding to a half-life time of 194 min. The product rate constants are then estimated to be $k_2 \sim 1.1 \times 10^{-5}$ s^{-1} and $k_4 \sim 4.9 \times 10^{-5}$ s^{-1} (see the Experimental and Computational Methods section in the main text for more details).
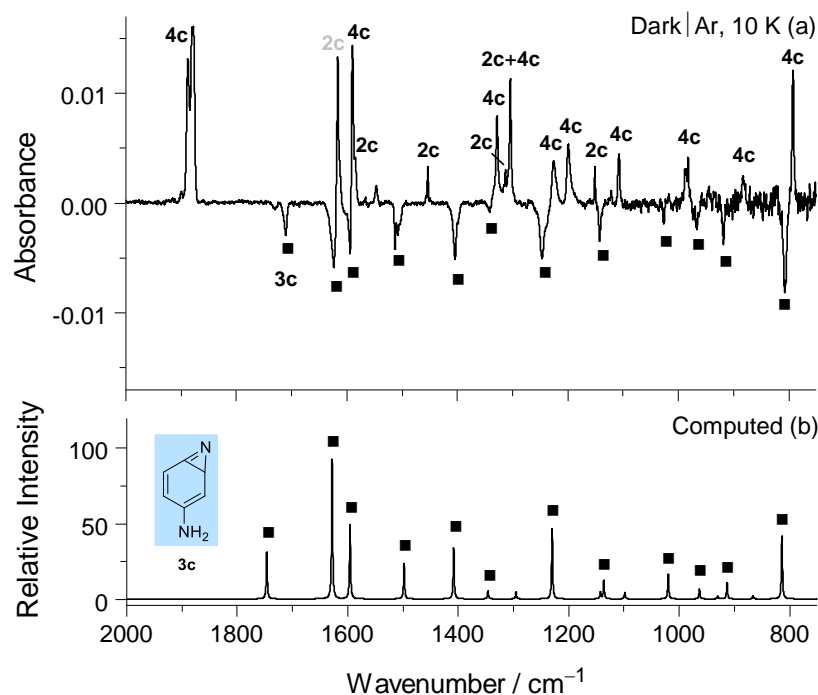
Figure S8. (a) Experimental difference IR spectrum showing changes after keeping the sample at 10 K (argon matrix) under dark conditions for 24 h, subsequent to irradiation at $\lambda = 435$ nm. The negative bands are due to the depletion of benzazirine **3c**. The positive bands are due the formation of triplet nitrene $^3A_2$-**2c** and ketenimine **4c**. The product $^3A_2$-**2c**:**4c** ratio is estimated roughly as 18:82 (see the Experimental and Computational Methods section in the main text for more details). To measure the kinetics of spontaneous rearrangement of **3c**, a few spectra were recorded (during this 24-hour period) while protecting the sample with an infrared long-pass cutoff filter transmitting only below 2200 cm^{-1} (see Figure S7). (b) IR spectrum of amino-substituted benzazirine **3c** computed at the B3LYP/6-311+G(2d,p) level of theory.
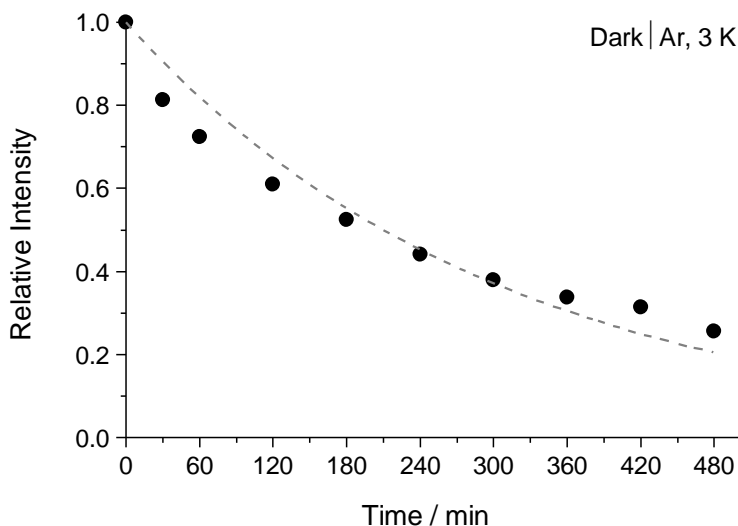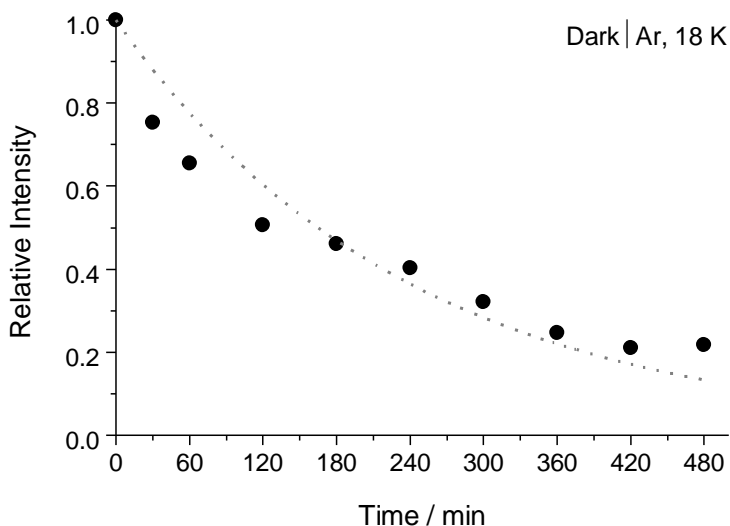
Figure S9. Kinetics of rearrangement of benzazirine **3c** to triplet nitrene $^3A_2$-**2c** and ketenimine **4c** in an argon matrix at 18 K under dark conditions. The spectra were recorded while protecting the sample with an infrared long-pass cutoff filter transmitting only below 2200 cm^{-1}. Black circles (●) represent the time evolution of the amount of **3c** (consumption, measured using the peak at 1710 cm^{-1}). The dotted line represents the best fit obtained using a first-order exponential decay kinetics equation. The rate constant obtained is $k_3 = 7.0 \times 10^{-5}$ s^{-1} corresponding to a half-life time of 165 min. The product rate constants are then estimated to be $k_2 \sim 1.2 \times 10^{-5}$ s^{-1} and $k_4 \sim 5.8 \times 10^{-5}$ s^{-1} (see the Experimental and Computational Methods section in the main text for more details).
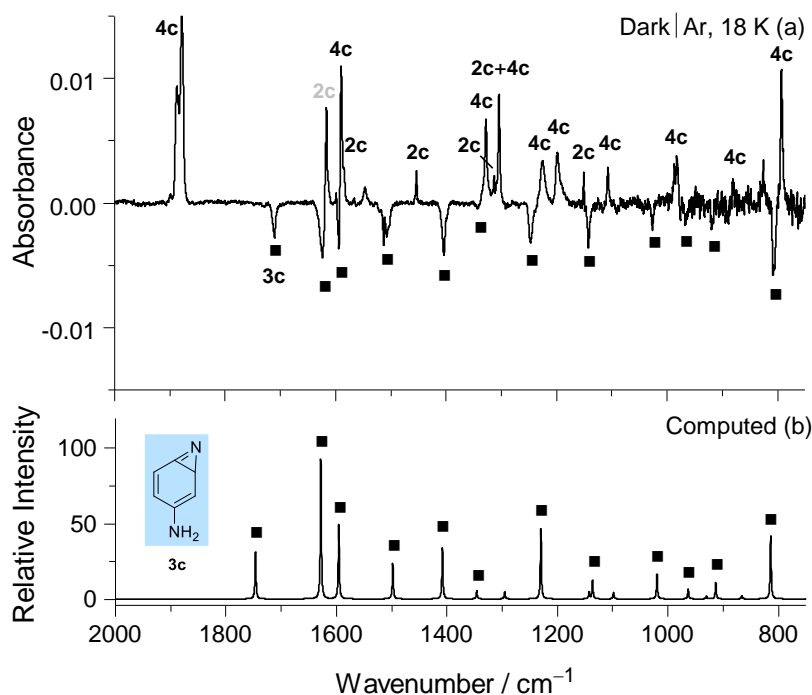
Figure S10. (a) Experimental difference IR spectrum showing changes after keeping the sample at 18 K (argon matrix) under dark conditions for 24 h, subsequent to irradiation at $\lambda = 435$ nm. The negative bands are due to the depletion of benzazirine **3c**. The positive bands are due to the formation of triplet nitrene $^3A_2$-**2c** and ketenimine **4c**. The product $^3A_2$-**2c**:**4c** ratio is estimated roughly as 17:83 (see the Experimental and Computational Methods section in the main text for more details). To measure the kinetics of spontaneous rearrangement of **3c**, a few spectra were recorded (during this 24-hour period) while protecting the sample with an infrared long-pass cutoff filter transmitting only below 2200 cm^{-1} (see Figure S9). (b) IR spectrum of amino-substituted benzazirine **3c** computed at the B3LYP/6-311+G(2d,p) level of theory.
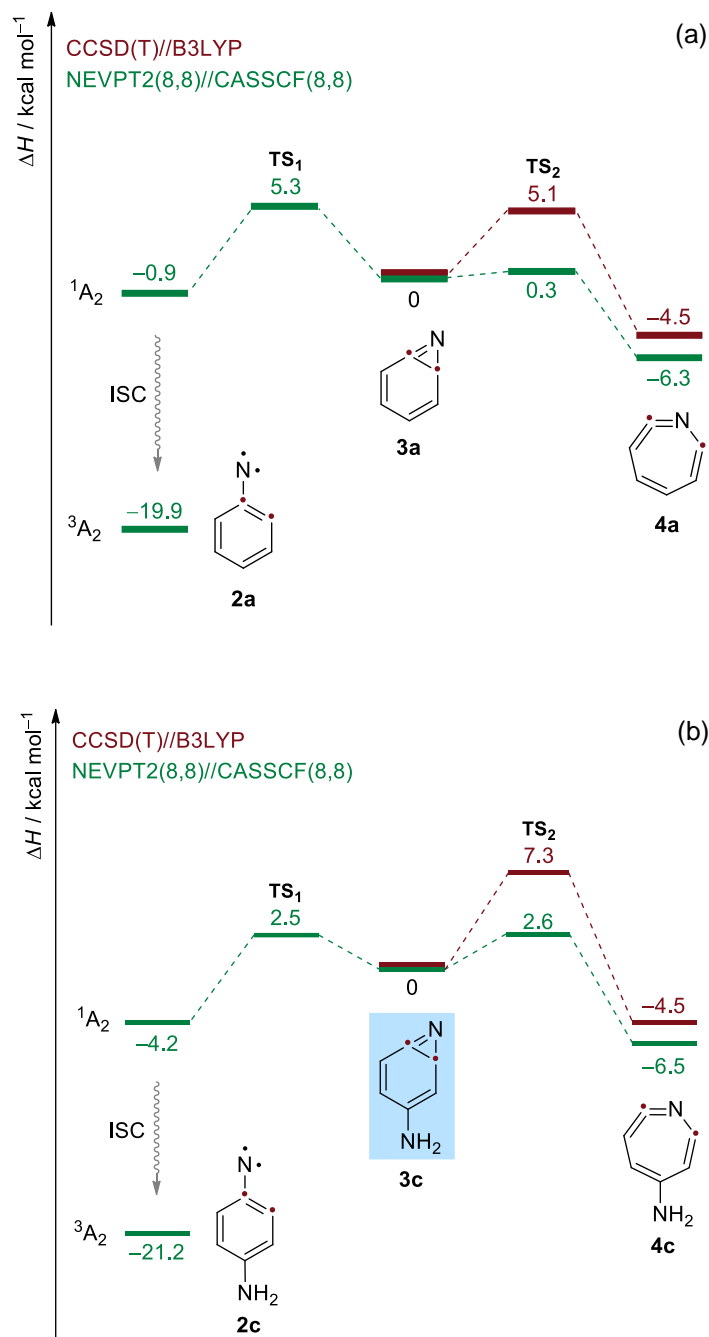
Figure S11. Energies of stationary points, including ZPVE corrections, on reaction pathways of **3a** (a) and **3c** (b) computed at CCSD(T)/cc-pVTZ//B3LYP/6-311+G(2d,p) (red) and NEVPT(8,8)/6-311+G(2d,p)//CASSCF(8,8)6-311+G(2d,p) (green) levels of theory. $^1A_2$ = open-shell singlet state, $^3A_2$ = triplet ground state, ISC = intersystem crossing, ZPVE = zero-point vibrational energy. Note that T_1 diagnostic (T_1= 0.028) indicates that **TS$_1$** cannot be computed adequately at CCSD(T) level of theory (or using other single-determinant wavefunction methodology), and therefore this method was only applied to compute the ring expansion of **3** to **4**.

Figure S12. Computed reaction path for nitrogen tunneling reaction of benzazirine **3c** to nitrene $^1A_2$-**2c** at NEVPT2/6-311+G(2d,p)//CASSCF(8,8)/6-311+G(2d,p) level of theory (see the Experimental and Computational Methods section in the main text for more details).
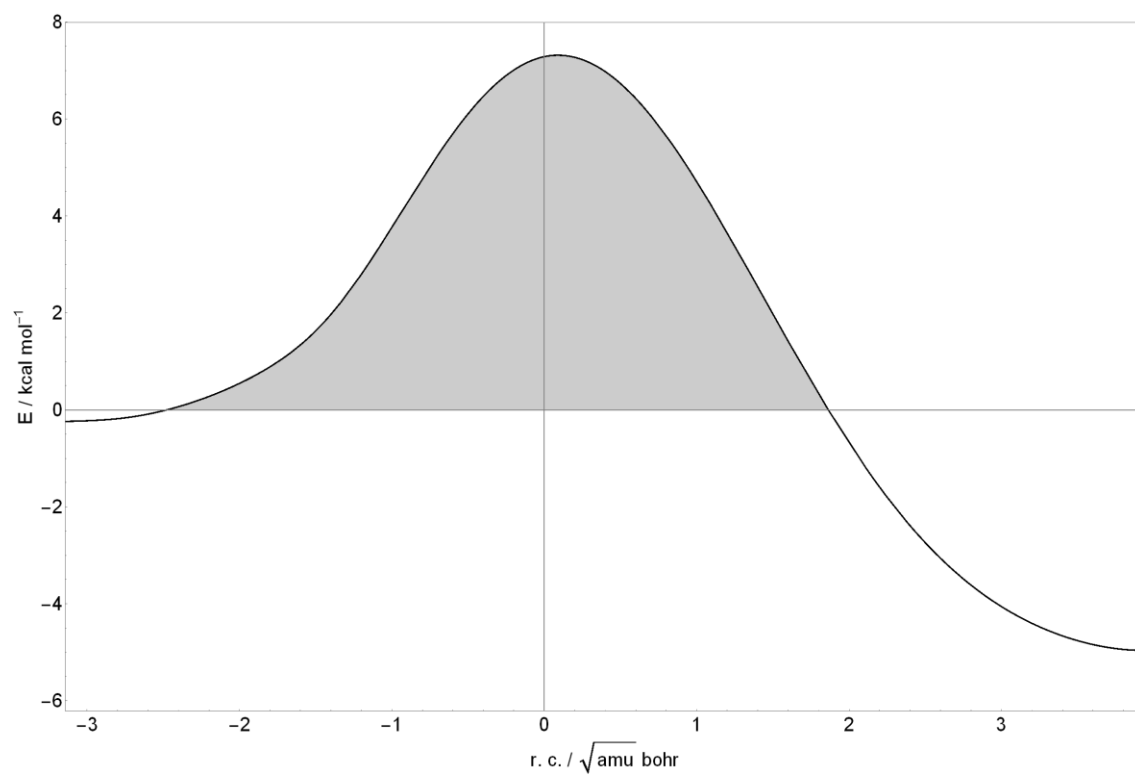
Figure S13. Computed reaction path for carbon tunneling reaction of benzazirine **3c** to cyclic ketenimine **4c** at CCSD(T)/cc-pVTZ//B3LYP/6-311+G(2d,p) level of theory (see the Experimental and Computational Methods section in the main text for more details).
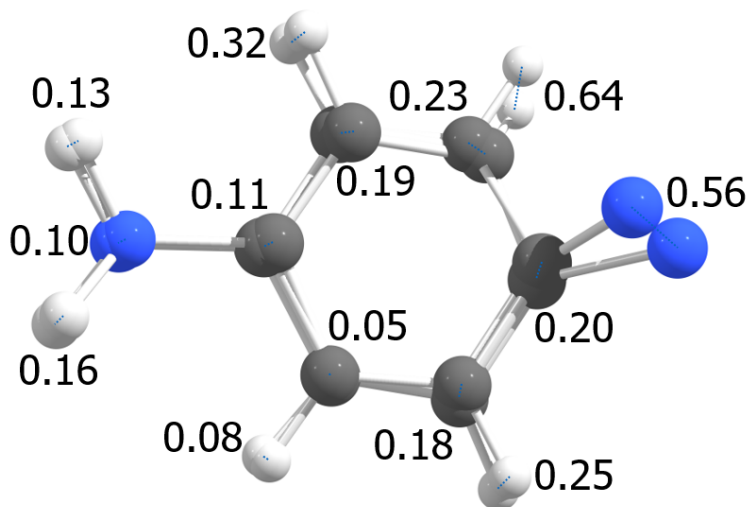
Figure S14a. Tunneling distances (arc lengths in Å) for every atom between the turning points (for the ring-opening tunneling reaction of **3c** to $^1A_2$-**2c**) computed at CASSCF(8,8)/6-311+G(2d,p) level of theory (see the Experimental and Computational Methods section in the main text for more details).
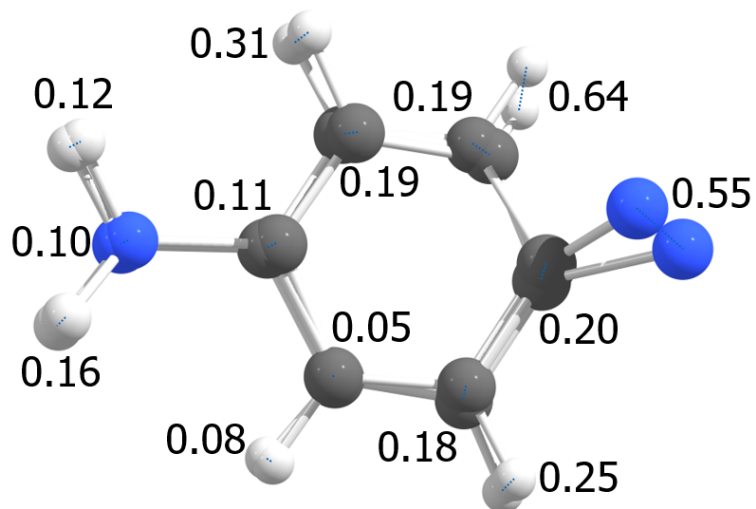
Figure S14b. Tunneling distances (Euclidian distances in Å) for every atom between the turning points (for the ring-opening tunneling reaction of **3c** to $^1A_2$-**2c**) computed at CASSCF(8,8)/6-311+G(2d,p) level of theory (see the Experimental and Computational Methods section in the main text for more details).
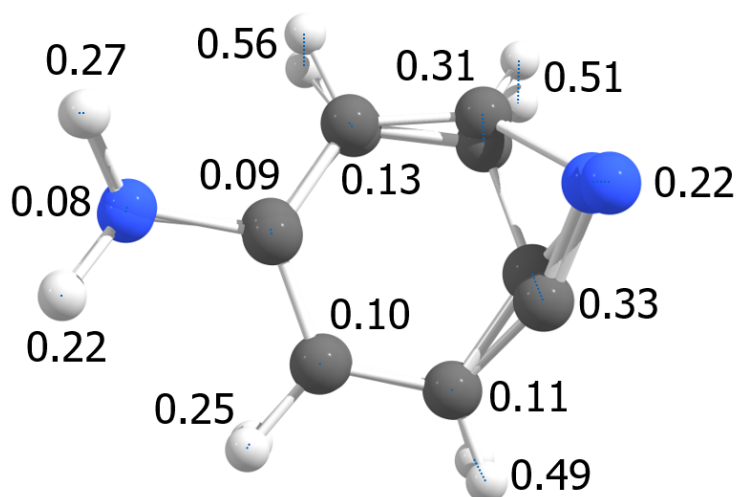
Figure S15a. Tunneling distances (arc lengths in Å) for every atom between the turning points (for the ring-expansion tunneling reaction of **3c** to **4c**) computed at B3LYP/6-311+G(2d,p) level of theory (see the Experimental and Computational Methods section in the main text for more details).
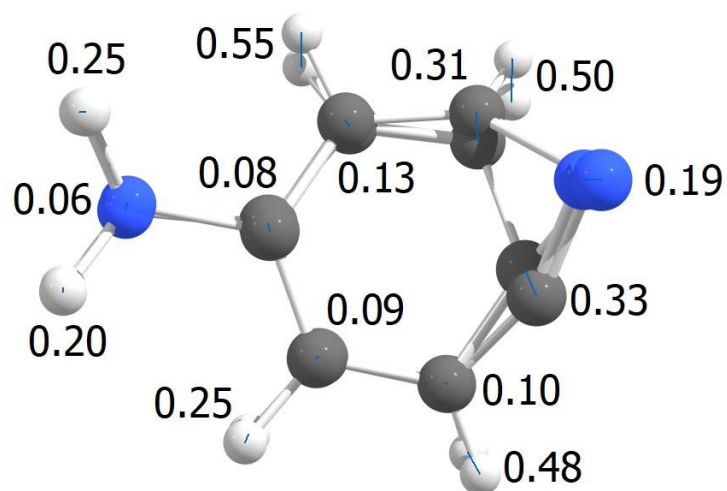
Figure S15b. Tunneling distances (Euclidian distances in Å) for every atom between the turning points (for the ring-expansion tunneling reaction of **3c** to **4c**) computed at B3LYP/6-311+G(2d,p) level of theory (see the Experimental and Computational Methods section in the main text for more details).
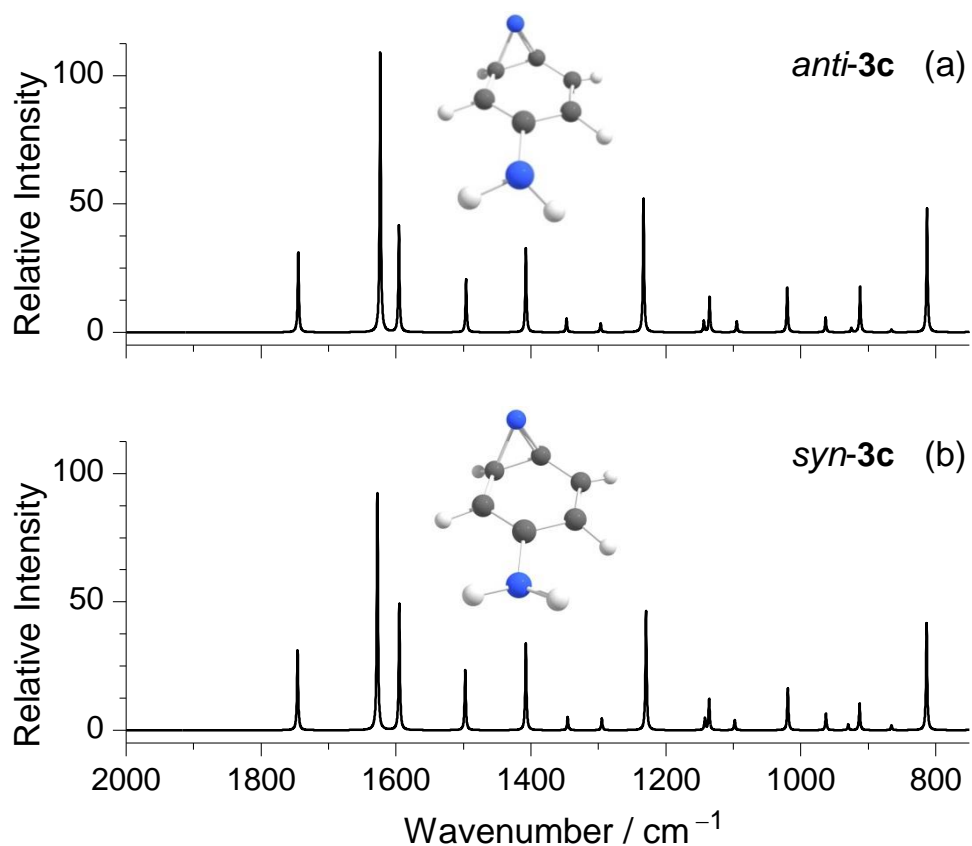
Figure S16. Computed IR spectra of two forms of amino-substituted benzazirine **3c**. The two forms differ in relative orientations of the amino group (with respect to the non-planar fused bicyclic ring). Computed B3LYP/6-311+G(2d,p) wavenumbers were scaled by 0.979 and convoluted with Lorentzian profiles having an FWHM of 2 cm^{-1}, with peak intensities equal to computed infrared intensities: (a) *anti*-**3c** form; (b) *syn*-**3c** form. Color codes: N − blue, C − gray, H − white. See Table S8 for more details.
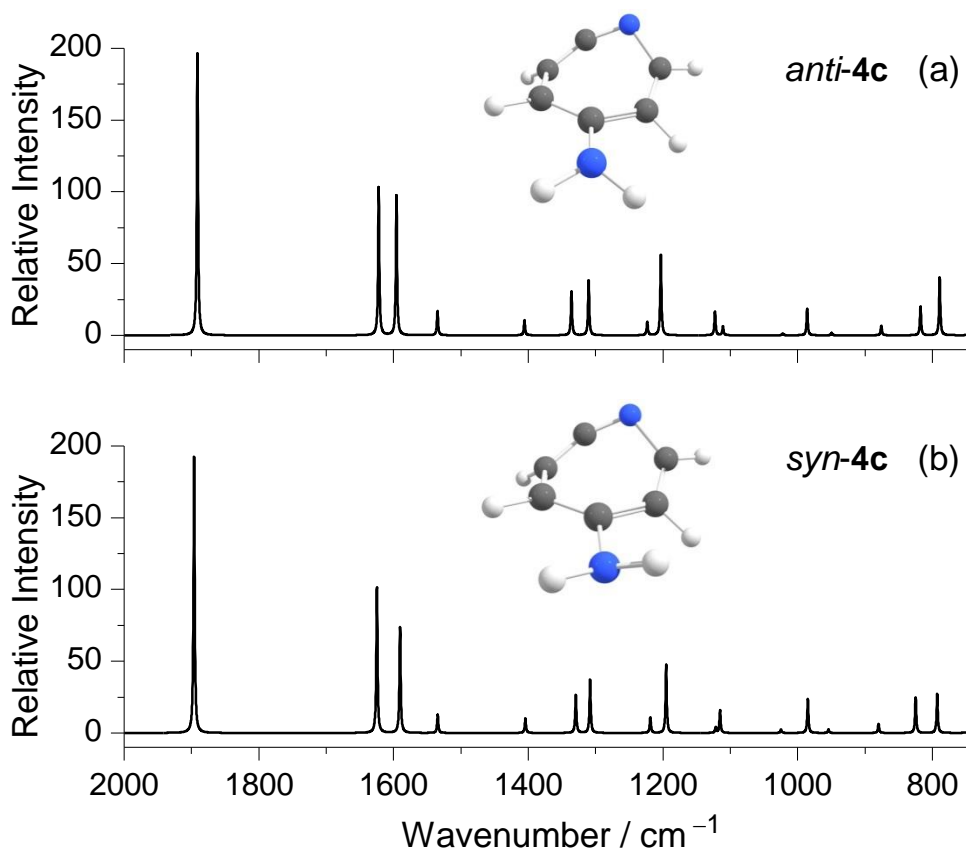
Figure S17. Computed IR spectra of two forms of amino-substituted cyclic ketenimine **4c**. The two forms differ in relative orientations of the amino group (with respect to the non-planar 7-membered ring). Computed B3LYP/6-311+G(2d,p) wavenumbers were scaled by 0.979 and convoluted with Lorentzian profiles having an FWHM of 2 cm^{-1}, with peak intensities equal to computed infrared intensities: (a) *anti*-**4c** form; (b) *syn*-**4c** form. Color codes: N – blue, C – gray, H – white. See Table S9 for more details.

III. Tables

Table S1. Experimental IR spectral data (argon matrix at 3 K), B3LYP/6-311+G(2d,p) computed vibrational frequencies (ν, cm^{-1}), absolute infrared intensities (A^{th}, km mol^{-1}), and vibrational assignment of p-azidoaniline **1c**.

Ar matrix[a]		Computed[b]		Approximate
ν	I	ν	A^{th}	assignment[c]
3501.5	m	3504	16.9	$\nu_{as}(NH_2)$
3415/3413	m/m	3414	24.0	$\nu_s(NH_2)$
3060	w	3063	3.5	$\nu(CH1)$
3046	w	3048	3.8	$\nu(CH2)$
3030	w	3034	14.7	$\nu(CH3)$
3016	w	3031	13.8	$\nu(CH4)$
2117/2080	vs/s	2161	946.5	$\nu_{as}(N_3)$
1628	m	1628	105.0	$\delta(NH_2) + \nu(Ring1)$
1612	m	1615	3.4	$\nu(Ring1) - \delta(NH_2)$
1592	m	1583	6.2	$\nu(Ring2)$
1512	vs	1511	221.6	$\nu(Ring3) + \delta(CH1)$
1439	vw	1443	1.5	$\nu(Ring4)$
1325	w	1334	29.4	$\delta(CH2) + \nu_s(N_3)$
1315/1314	m/m	1325	74.0	$\nu_s(N_3) - \delta(CH2)$
1304	m	1297	9.2	$\nu(Ring5)$
1283/1274	s/s	1269	137.1	$\nu(CN_A) - \delta(CH1)$
1179.5	m	1180	10.1	$\delta(CH3)$
1134	w	1130	4.1	$\delta(CH4) + \nu(CN_{N3})$
1126	m	1127	13.4	$\nu(CN_{N3}) - \delta(CH4)$
1062/1059	w/w	1063	4.0	$\gamma(NH_2)$
		1006	0.1	$\delta(Ring1)$
		930	0.3	$\gamma(CH1)$
		911	0.2	$\gamma(CH2)$
848	vw	838	3.4	$\nu(Ring6)$
829/821	m/m	818	69.2	$\gamma(CH3)$
804/801	w	793	3.1	$\gamma(CH4)$
779	w	772	9.5	$\delta(CNN) - \delta(NNN1)$
697	w	703	3.5	$\tau(Ring1)$
643	w	643	1.4	$\delta(Ring2)$
640/637	m/m	640	8.0	$\delta(NNN1)$
429	vs	586	347.1	$\omega(NH_2)$
530	w	529	8.8	$\delta(NNN2)$
507/504	m/m	498	59.1	$\tau(Ring2)$
435	w	434	1.8	$\delta(CCN_{N3}) - \delta(CCN_A) - \delta(Ring3)$
		413	0.2	$\tau(Ring3)$
		409	0.04	$\delta(Ring3) + \delta(CCN_A) - \delta(CCN_{N3})$
		341	6.6	$\gamma(CN_{N3}) - \gamma(CN_A)$
		318	1.7	$\delta(CCN_A) + \delta(CCN_{N3})$
		267	19.3	$\tau(NH_2)$
		151	1.3	$\gamma(CN_A) + \gamma(CN_{N3})$
		127	0.8	$\delta(NNN3)$
		59	0.3	$\tau(CCNN)$

[a]Experimental intensities are presented in qualitative terms: vs = very strong, s = strong, m = medium, w = weak, vw = very weak. [b]Computed harmonic frequencies were scaled by 0.960 and 0.979, above and below 3000 cm^{-1}, respectively. [c]Assignments made by inspection of Chemcraft animations. Abbreviations: ν = stretching, δ = bending, γ = rocking, ω = wagging, τ = torsion, s = symmetric, as = antisymmetric, N_A = nitrogen atom from the Amino group, N_{N3} = nitrogen atom from the N$_3$ (azide) group, adjacent to carbon atom. Signs "+" and "−" designate combinations of vibrations occurring in "syn"-phase ("+") and in "anti"-phase ("−").

Table S2. Experimental IR spectral data (argon matrix at 3 K), B3LYP/6-311+G(2d,p) computed vibrational frequencies (ν, cm^{-1}), absolute infrared intensities (Ath, km mol^{-1}), and vibrational assignment of amino-substituted ketenimine **4c**.[a]

Ar matrix[b]		Computed[c]		Approximate assignment[d]
ν	I	ν	Ath	
3486/3482	w/w	3494	15.4	$\nu_{as}(NH_2)$
3399/3394	w/w	3403	14.1	$\nu_s(NH_2)$
1887/1878	s/s	1896	194.3	$\nu_{as}(C=C=N)$
1624/1608	ov	1625	101.9	$\delta(NH_2)$
1590	m/ov	1590	74.5	$\nu_{as}(C=C)$
1547/1539	w/vw	1534	12.7	$\nu_s(C=C)$
1401	w	1404	10.4	$\delta(CH1)$
1327	m (ov)	1329	26.6	$\delta(CH2)$
1303	m (ov)	1308	37.3	$\delta(CH3)$
1225	w (br)	1219	10.9	$\delta(CH4)$
1199	w (br)	1195	47.7	$\nu(CN_A)$
-	ov	1122	3.9	$\gamma(NH_2) - \nu(C-C1)$
1106	w	1115	15.7	$\nu_s(C=C=N)$
-	-	1025	2.4	$\nu(C-C1) + \gamma(NH_2)$
986/982	w/w	985	23.7	$\nu(CN_R)$
-	-	954	2.3	$\gamma(CH1)$
883	vw	880	6.2	$\gamma(CH2)$
826	ov	825	25.0	$\gamma(CH3)$
792	s	793	27.2	$\gamma(CH4)$
737	w	736	27.2	$\nu(C-C2) + \delta(Ring1)$
689	m	697	49.6	$\tau(Ring1)$
667	m	671	17.5	$\gamma(CH1)$
*	-	636	76.6	$\tau(Ring2) - \omega(NH_2)$
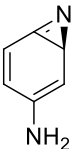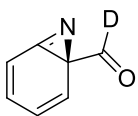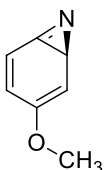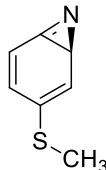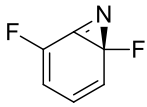
[a]Amino-substituted ketenimine **4c** was generated during irradiation of triplet *p*-aminophenylnitrene $^3A_2$-**2c** in an argon matrix at 3 K. [b]Experimental intensities are presented in qualitative terms: s = strong, m = medium, w = weak, vw = very weak, br = broad, and ov = overlapped. [c]Computed harmonic frequencies were scaled by 0.960 and 0.979, above and below 3000 cm^{-1}, respectively. [d]Assignments made by inspection of Chemcraft animations. Abbreviations: ν = stretching, δ = bending, γ = rocking, ω = wagging, τ = torsion, s = symmetric, as = antisymmetric, N$_A$ = nitrogen atom from the Amino group, N$_R$ = nitrogen atom from the ketenimine Ring. Signs "+" and "−" designate combinations of vibrations occurring in "syn"-phase ("+") and in "anti"-phase ("−"). *It is difficult to assign the theoretical modes [$\tau(Ring2) - \omega(NH_2)$] and [$\omega(NH_2) + \tau(Ring2)$]. In the experiments, the bands due to these very anharmonic vibration modes of **4c** probably appear below 600 cm^{-1}. The bands shown in bold (the most intense bands of **4c**) are those that were observed in the experiments as result of the spontaneous rearrangement of **3c** in the dark (IR spectrum was collected using a cutoff filter transmitting below 2200 cm^{-1}).

Table S3. Experimental IR spectral data (argon matrix at 3 K), B3LYP/6-311+G(2d,p) computed vibrational frequencies (ν, cm^{-1}), absolute infrared intensities (A^{th}, km mol^{-1}), and vibrational assignment of triplet p-aminophenylnitrene $^3A_2$-**2c**.[a]

Ar matrix[b]		Computed[c]			Approximate assignment[d]
ν	I	ν	A^{th}	Sym.	
3547/3540/3533/3527	vw/vw/w/w	3525	25.3	A"	$\nu_{as}(NH_2)$
3443/3439/3434/3429	m/w/m/m	3427	51.3	A'	$\nu_s(NH_2)$
1616	s	1623	135.4	A'	$\delta(NH_2)$
1588/1584*	w/m	1586	139.4	A'	$\nu(Ring1)$
-	-	1510	0.1	A"	$\nu(Ring2)$
1453	m	1452	27.8	A'	$\nu(Ring3) - \nu(CN_A)$
-	-	1425	1.8	A"	$\delta(CH1)$
1321	w	1317	5.4	A"	$\delta(CH2)$
1312	m	1305	16.7	A'	$\nu(CN_N)$
1308/1306	w/m	1292	80.9	A'	$\nu(CN_A) + \nu(Ring3)$
1239	vw	1234	3.0	A"	$\nu(Ring4)$
1154/1151	w/m	1150	35.3	A'	$\delta(CH3)$
1120	w	1121	11.1	A"	$\delta(CH4)$
-	-	1037	0.3	A"	$\gamma(NH_2)$
-	-	968	0.5	A'	$\nu(Ring5)$
-	-	927	0.0	A"	$\gamma(CH1)$
-	-	922	0.1	A'	$\gamma(CH2)$
-	-	821	0.8	A'	$\nu(Ring6)$
817/807	w/vw	807	66.3	A'	$\gamma(CH3)$
-	-	773	0.1	A"	$\gamma(CH4)$
773/769	vw/w	763	8.3	A'	$\delta(Ring1)$
-	-	702	0.6	A'	$\tau(Ring1)$
-	-	626	0.3	A"	$\delta(Ring2)$

[a]Triplet p-aminophenylnitrene $^3A_2$-**2c** was generated by irradiation of p-azidoaniline **1c** at $\lambda = 254$ nm in an argon matrix at 3 K. Experimental intensities are presented in qualitative terms: s = strong, m = medium, w = weak, vw = very weak, br = broad, and ov = overlapped. [c]Computed harmonic frequencies were scaled by 0.960 and 0.979, above and below 3000 cm^{-1}, respectively. [d]Assignments made by inspection of Chemcraft animations. Abbreviations: ν = stretching, δ = bending, γ = rocking, ω = wagging, τ = torsion, s = symmetric, as = antisymmetric, N_A = nitrogen atom from the Amino group, N_N = nitrogen atom from the Nitrene group. Signs "+" and "−" designate combinations of vibrations occurring in "syn"-phase ("+") and in "anti"-phase ("−"). *1574/1566 cm^{-1} (~vw/vw) experimental observed bands not mentioned in the table are difficult to assign. The bands shown in bold (the most intense bands of $^3A_2$-**2c**) are those that were observed in the experiments as result of the spontaneous rearrangement of **3c** in the dark (IR spectrum was collected using a cutoff filter transmitting below 2200 cm^{-1}).

Table S4. Comparison of the experimental and B3LYP/6-311+G(2d,p) calculated ν(C=N) vibrational frequencies (cm^{-1}) of some known benzazirines.

Structure						
Exp.[a]	1710[this work]	1751[1]	1731[2]	1717[3]	1716[3]	1679[4]
Cal.[b]	1746	1785	1754	1747	1752	1706
Δ[Cal.-Exp.][c]	+36	+34	+23	+30	+36	+27

[a]Corresponding to benzazirines isolated in argon matrices: See refs. [1-4]. [b]All calculated frequencies (cm^{-1}) were scaled by a common factor of 0.979. If more than one conformer is possible then the most stable conformer is shown. [c]The "calculated" minus "experimental" difference is taken for the most stable calculated conformer.

Table S5. Experimental IR spectral data (argon matrix at 3 K), B3LYP/6-311+G(2d,p) computed vibrational frequencies (v, cm^{-1}), absolute infrared intensities (A^{th}, km mol^{-1}), and vibrational assignment of amino-substituted benzazirine **3c**.[a]

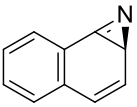| Ar matrix[b]		Computed[c]		Approximate assignment[d]
v	I	v	A^{th}	
3487/3482	m/m	3494	16.7	$v_{as}(NH_2)$
3403/3399	m/m	3407	16.8	$v_s(NH_2)$
1710	m	1746	31.3	$v(C=N_R)$
1626/1623	sh/s (ov)	1628	92.3	$\delta(NH_2)$
1593	s (ov)	1595	49.6	$v_{as}(C=C)$
1508/1503	m/sh	1497	23.4	$v_s(C=C)$
1403	s	1407	34.1	$\delta(CH1)$
1340	w	1345	5.2	$\delta(CH2)$
-	ov?	1295	4.5	$\delta(CH3)$
1246	m	1229	46.9	$v(CN_A)$
-	ov?	1142	4.6	$\delta(CH4)$
1142	m	1136	12.1	$v(C-C1)$
-	ov?	1098	3.9	$\gamma(NH_2)$
1026	m	1019	16.4	$v(C-C2)$
968	w	963	6.5	$v(C-C3)$
931	vw	930	2.2	$\gamma(CH1)$
917	m	913	10.6	$\gamma(CH2)$
-	-	866	1.9	$v(C-C4)$
806	s	813	41.8	$\gamma(CH3)$
742	w	742	4.5	$\delta(Ring1)$
727/708	w/br	716	11.6	$\gamma(CH4)$
*	w/br	658	156.1	$\omega(NH_2)$
628	w/br	627	11.8	$\tau(Ring2)$
607	w/br	595	16.3	$\delta(Ring2)$

[a]Amino-substituted benzazirine **3c** was generated during irradiation of triplet p-aminophenylnitrene $^3A_2$-**2c** at $\lambda = 436$ nm in an argon matrix at 3 K. [b]Experimental intensities are presented in qualitative terms: s = strong, m = medium, w = weak, vw = very weak, br = broad, and ov = overlapped. [c]Computed harmonic frequencies were scaled by 0.960 and 0.979, above and below 3000 cm^{-1}, respectively. [d]Assignments made by inspection of Chemcraft animations. Abbreviations: v = stretching, δ = bending, γ = rocking, ω = wagging, τ = torsion, s = symmetric, as = antisymmetric, N_A = nitrogen atom from the Amino group, N_R = nitrogen atom from the benzazirine Ring. Signs "+" and "−" designate combinations of vibrations occurring in "syn"-phase ("+") and in "anti"-phase ("−"). *It is difficult to assign the theoretical modes $\omega(NH_2)$. In the experiment, the band due to this very anharmonic vibration mode of **3c** probably appears below 600 cm^{-1} [compare with the $\omega(NH_2)$ mode of **1c**, Figure S1, part 4].

Table S6. WKB-tunneling analysis for the reaction of benzazirine **3c** to nitrene $^1A_2$-**2c**.[a]

Tunneling parameters	NEVPT2/6-311+G(2d,p)// CASSCF(8,8)/6-311+G(2d,p)
Collision energy (ε, kcal mol^{-1})	0.2
Collision frequency (ω_0, cm^{-1})	164
Barrier (kcal mol^{-1})	2.5
Effective barrier (kcal mol^{-1})	2.7
Turning points [(s1, s2), amu$^{1/2}$ bohr]	–2.21, 2.81
Barrier penetration integral (θ)	17.74
WKB transmission probability (κ_{WKB})	3.88×10^{-14}
WKB half-life time (τ_{WKB})	6 min

[a]See also Figures S12 and S14.

Table S7. WKB-tunneling analysis for the reaction of benzazirine **3c** to ketenimine **4c**.[a]

Tunneling parameters	CCSD(T)cc-pVTZ// B3LYP/6-311+G(2d,p)
Collision energy (ε, kcal mol^{-1})	0.2
Collision frequency (ω_0, cm^{-1})	167
Barrier (kcal mol^{-1})	7.3
Effective barrier (kcal mol^{-1})	7.5
Turning points [(s1, s2), amu$^{1/2}$ bohr]	–2.48, 1.86
Barrier penetration integral (θ)	18.63
WKB transmission probability (κ_{WKB})	6.59×10^{-15}
WKB half-life time (τ_{WKB})	35 min

[a]See also Figures S13 and S15

Table S8. B3LYP/6-311+G(2d,p) computed vibrational frequencies (v, cm^{-1}) and absolute infrared intensities (A^{th}, km mol^{-1}) of the two forms of amino-substituted benzazirine **3c**. [a]

syn-**3c**		anti-**3c**		Difference
v	A^{th}	v	A^{th}	Δv
3639.6	16.7	3640.1	13.2	-0.5
3548.5	16.8	3544.2	11.5	4.3
3202.3	2.2	3201.2	2.4	1.1
3162.1	4.0	3155.2	2.8	6.9
3155.2	24.3	3154.4	27.7	0.9
3135.2	19.9	3134.3	21.1	0.9
1783.3	**31.3**	**1782.3**	**31.3**	**1.0**
1662.5	92.3	1658.1	109.7	4.4
1629.3	49.6	1629.8	41.6	-0.5
1529.5	23.4	1528.2	20.7	1.3
1437.7	34.1	1437.7	32.9	0.0
1374.3	5.2	1376.1	5.4	-1.8
1322.6	4.5	1324.4	3.5	-1.8
1255.7	46.9	1259.5	52.1	-3.8
1166.6	4.6	1168.1	4.3	-1.6
1160.2	12.1	1159.5	13.9	0.7
1121.4	3.9	1118.3	4.2	3.0
1041.0	16.4	1042.0	17.5	-1.0
983.3	6.5	983.7	5.7	-0.5
949.5	2.2	944.7	1.7	4.8
932.4	10.6	931.6	17.9	0.7
884.1	1.9	884.1	1.1	-0.1
830.8	41.8	830.2	48.3	0.6
758.1	4.5	762.8	2.4	-4.7
730.9	11.6	732.5	25.2	-1.6
672.2	*156.1*	*627.7*	*111.3*	*44.5*
640.9	11.8	641.5	5.8	-0.6
607.7	16.3	602.0	18.9	5.7
588.1	*140.8*	*607.6*	*120.2*	*-19.5*
530.1	7.5	528.4	7.1	1.8
437.3	11.2	435.4	29.5	1.9
387.7	3.2	392.8	4.2	-5.1
375.2	2.6	374.0	12.0	1.2
285.4	5.8	293.4	36.8	-8.0
270.9	40.0	274.4	10.7	-3.6
163.8	9.3	166.0	2.9	-2.2

[a]Frequencies not scaled. In the 2000–700 cm^{-1} spectral range used for vibrational assignments, the mean absolute difference in vibrational frequencies (syn-**3c** minus anti-**3c**) is below 2 cm^{-1}. The characteristic stand-alone mode v(C=N) used for kinetic measurements is shown in bold. The very anharmonic modes with strong contributions of ω(NH$_2$) are shown in italic.

Table S9. B3LYP/6-311+G(2d,p) computed vibrational frequencies (ν, cm^{-1}) and absolute infrared intensities (A^{th}, km mol^{-1}) of the two forms of amino-substituted ketenimine **4c**. [a]

syn-**4c**		anti-**4c**		Difference
ν	A^{th}	ν	A^{th}	$\Delta\nu$
3639.8	*15.4*	*3659.0*	*16.3*	*-19.2*
3544.5	*14.1*	*3559.9*	*20.1*	*-15.4*
3189.3	5.1	3188.3	5.0	1.0
3175.0	19.3	3171.4	21.3	3.6
3151.2	1.8	3137.6	6.3	13.5
3114.8	32.9	3113.9	32.9	0.9
1936.8	**194.3**	**1931.7**	**196.8**	**5.0**
1659.5	101.9	1656.8	103.1	2.7
1624.4	74.5	1629.9	97.6	-5.4
1567.3	12.7	1567.6	17.1	-0.3
1434.4	10.4	1435.7	10.6	-1.4
1357.9	26.6	1364.5	30.4	-6.6
1336.2	37.3	1338.4	38.7	-2.2
1244.9	10.9	1249.5	9.5	-4.6
1220.8	47.7	1228.9	56.6	-8.1
1145.7	3.9	1146.8	16.8	-1.1
1139.1	15.7	1134.7	6.3	4.5
1046.6	2.4	1044.0	1.3	2.6
1005.9	23.7	1007.0	18.5	-1.0
974.6	2.3	969.9	1.6	4.8
898.7	6.2	894.5	6.8	4.2
842.4	25.0	835.0	20.3	7.4
809.8	27.2	806.0	40.6	3.8
752.2	27.2	750.4	20.9	1.8
711.9	49.6	717.6	38.5	-5.7
685.2	17.5	682.3	18.8	2.8
649.8	*76.6*	*626.6*	*17.0*	*23.1*
610.8	*173.3*	*567.9*	*157.6*	*42.9*
530.1	30.1	526.4	59.2	3.7
472.5	15.1	472.0	57.4	0.5
442.9	7.9	441.9	30.4	1.1
384.8	3.4	378.3	10.6	6.5
359.0	13.5	361.3	15.8	-2.3
320.7	41.8	297.9	5.7	22.8
294.3	8.1	281.1	17.1	13.2
173.0	5.7	170.2	1.1	2.8

[a]Frequencies not scaled. In the 2000–700 cm^{-1} spectral range used for vibrational assignments, the mean absolute difference in vibrational frequencies (*syn*-**4c** minus *anti*-**4c**) is below 4 cm^{-1}. The characteristic stand-alone mode ν_{as}(C=C=N) used for kinetic measurements is shown in bold. The very anharmonic modes with strong contributions of ν(NH$_2$) and ω(NH$_2$) are shown in italic.

IV. Computed Data

Optimized geometries (Cartesian coordinates, Å), electronic energies (E_h, in hartree) and zero-point vibrational energy (ZPVE, in hartree) computed at B3LYP/6-311+G(2d,p) level of theory for species **1c**-**4c** and **TS2**.

1c (E_h = −451.331111; ZPVE = 0.119432)

C	1.137296	-1.203523	-0.007422
C	2.094974	-0.183732	-0.005696
C	1.648267	1.143306	-0.003929
C	0.295315	1.438974	-0.000465
C	-0.650952	0.415441	-0.000550
C	-0.218602	-0.910645	-0.004186
H	1.457291	-2.239769	-0.015573
H	2.370920	1.951950	-0.009284
H	-0.042312	2.467680	0.003048
H	-0.936580	-1.722725	-0.003663
N	-2.017964	0.810307	0.004686
N	-2.884399	-0.061255	0.004306
N	-3.768504	-0.768659	0.004529
N	3.459851	-0.480865	-0.071264
H	4.072349	0.239204	0.283638
H	3.717660	-1.391954	0.279525

$^3A_2$-2c (E_h = −341.771986; ZPVE = 0.107562)

C	0.002636	-1.551600	0.000000
C	0.000041	1.286784	0.000000
C	0.003331	-0.803951	1.224061
C	0.003331	-0.803951	-1.224061
C	0.003331	0.568050	1.212563
C	0.003331	0.568050	-1.212563
H	0.007870	1.112978	-2.150859
H	0.007870	1.112978	2.150859
H	0.002610	-1.348773	2.159294
H	0.002610	-1.348773	-2.159294
N	0.000001	-2.867686	0.000000
N	0.051932	2.669555	0.000000
H	-0.240244	3.139106	-0.843372
H	-0.240244	3.139106	0.843372

anti-**3c** (E$_h$ = −341.734838; ZPVE = 0.107817), See Fig. S16(a)

```
N        -2.039884   -0.466294    0.755783
C        -1.521893    0.348037   -0.049194
C        -0.729175    1.535983   -0.175397
C         0.591486    1.244380   -0.096750
C        -1.118796   -1.013052   -0.419219
C         0.304205   -1.207996   -0.204205
C         1.104808   -0.117677    0.011202
H        -1.119142    2.535728   -0.308530
H         1.315263    2.053134   -0.107443
H        -1.654679   -1.582755   -1.168333
H         0.756747   -2.187293   -0.333138
N         2.468247   -0.234962    0.307782
H         3.056484    0.500471   -0.058047
H         2.862982   -1.148546    0.131906
```


syn-**3c** (E$_h$ = −341.735312; ZPVE = 0.107883), See Fig. S16(b)

```
N        -2.036675   -0.466685    0.765169
C        -1.521233    0.348288   -0.040302
C        -0.728244    1.536644   -0.169962
C         0.592597    1.243712   -0.113484
C        -1.121068   -1.010359   -0.418054
C         0.300637   -1.210029   -0.195094
C         1.104845   -0.119382    0.003317
H        -1.119247    2.536011   -0.302323
H         1.321441    2.045648   -0.163202
H        -1.661484   -1.578157   -1.165245
H         0.749807   -2.192776   -0.308386
N         2.495635   -0.229633    0.148264
H         2.814317   -1.150194    0.415656
H         2.917244    0.480454    0.730946
```

TS2 (E_h = −341.7252509; ZPVE = 0.106224; i= 521.9 cm^{-1})

C	−0.770458000	1.545569000	−0.253539000
C	−1.551244000	0.471374000	0.073723000
C	−1.110880000	−1.159483000	−0.330201000
C	0.278498000	−1.169963000	−0.321127000
C	1.079399000	−0.066022000	0.032250000
C	0.584669000	1.245446000	−0.060902000
H	−1.139822000	2.474071000	−0.663605000
H	0.783437000	−2.004135000	−0.800537000
H	1.299379000	2.063439000	−0.070670000
N	−1.900195000	−0.498861000	0.763618000
H	−1.690928000	−1.765013000	−1.016548000
N	2.472003000	−0.280655000	0.163162000
H	2.981435000	0.542422000	0.454310000
H	2.703936000	−1.055695000	0.768367000

anti-**4c** (E_h = −341.746032; ZPVE = 0.107859), See Fig. S17(a)

N	−1.851910	−0.495325	−0.561812
C	−1.036121	−1.415747	0.141360
C	0.268078	−1.169567	0.391020
C	1.061269	0.017127	0.033347
C	0.592963	1.299859	−0.007891
C	−0.800528	1.585568	0.335923
C	−1.590618	0.654588	−0.160458
H	1.261725	2.097771	−0.323457
H	−1.486586	−2.368432	0.397321
H	0.832655	−1.995772	0.813809
H	−1.124297	2.388699	0.983242
N	2.387071	−0.266777	−0.309843
H	3.034821	0.504211	−0.236105
H	2.765294	−1.122730	0.066967

syn-**4c** (E_h = −341.747160; ZPVE = 0.108091), See Fig. S17(b)

N	−1.848426	−0.494064	−0.567203
C	−1.036140	−1.416464	0.140074
C	0.266033	−1.169282	0.400237
C	1.059114	0.015843	0.040050
C	0.590400	1.296491	−0.026097
C	−0.801082	1.589518	0.329734
C	−1.586700	0.653549	−0.161465
H	1.256732	2.090592	−0.355689
H	−1.490101	−2.367932	0.393587
H	0.833847	−1.982177	0.841311
H	−1.122258	2.392040	0.978995
N	2.419764	−0.264940	−0.151000
H	2.613708	−1.134396	−0.628453
H	2.958962	0.496967	−0.537520

Optimized geometries (Cartesian coordinates, Å), electronic energies (E$_h$, in hartree) and zero-point vibrational energy (ZPVE, in hartree) computed at CASSCF(8,8)/6-311+G(2d,p) level of theory for PES around **3a**.

^{3}A$_2$-**2a** (E$_h$ = -284.6668044; ZPVE = 0.094697)

```
C       -1.047812000       1.213150000      -0.000003000
C        0.333763000       1.225761000      -0.000014000
C        1.053041000       0.000038000      -0.000062000
C        0.333820000      -1.225721000      -0.000020000
C       -1.047754000      -1.213180000      -0.000003000
C       -1.746976000      -0.000031000      -0.000006000
H       -1.589014000       2.141033000       0.000033000
H        0.880680000       2.149549000       0.000024000
H        0.880787000      -2.149479000       0.000013000
H       -1.588910000      -2.141090000       0.000032000
H       -2.820644000      -0.000056000       0.000029000
N        2.386809000       0.000051000       0.000070000
```

^{1}A$_2$-**2a** (E$_h$ = -284.6393944; ZPVE = 0.093924)

```
C       -1.036278000       1.231547000       0.000074000
C        0.325165000       1.257628000       0.000184000
C        1.086714000       0.000035000       0.000919000
C        0.325225000      -1.257593000       0.000186000
C       -1.036219000      -1.231577000       0.000069000
C       -1.748527000      -0.000032000       0.000179000
H       -1.586642000       2.154284000      -0.000263000
H        0.873774000       2.179263000      -0.000167000
H        0.873877000      -2.179203000      -0.000168000
H       -1.586540000      -2.154340000      -0.000265000
H       -2.820836000      -0.000057000      -0.000056000
N        2.358076000       0.000067000      -0.000600000
```


TS1 (E$_h$ = -284.626647; ZPVE = 0.093541; i = 216.9 cm^{-1})

```
N        0.005030000      -0.019562000       0.007325000
C       -0.001597000       0.005987000       1.261829000
C        1.043507000       0.005295000       2.291512000
C        1.002988000       1.051864000       3.140262000
C       -1.249897000       0.715691000       1.498310000
C       -1.120870000       1.938886000       2.234346000
C       -0.028054000       2.090084000       3.036160000
H        1.810564000      -0.744082000       2.319604000
H        1.753811000       1.160462000       3.900985000
H       -2.156222000       0.385422000       1.040807000
H       -1.907264000       2.671068000       2.234864000
H        0.072001000       2.963286000       3.653112000
```

3a (E$_h$ = -284.6346237; ZPVE = 0.095533)

```
N        0.003292000      -0.006558000       0.005163000
C        0.002989000       0.007722000       1.257291000
C        0.908549000       0.003367000       2.397440000
C        1.247046000       1.261742000       2.748823000
C       -0.885968000       1.060607000       0.858743000
C       -0.300130000       2.381429000       1.149542000
C        0.715768000       2.442257000       2.042678000
H        1.278272000      -0.881058000       2.876274000
H        1.941014000       1.429364000       3.551931000
H       -1.945746000       0.924147000       0.772576000
H       -0.709147000       3.281694000       0.727016000
H        1.143352000       3.394416000       2.298646000
```

TS2 (E$_h$ = -284.6031118; ZPVE = 0.094029; i = 776.8 cm^{-1})

```
N        0.004971000      -0.001740000       0.006030000
C        0.003730000       0.009021000       1.247834000
C        0.744584000       0.001433000       2.412149000
C        1.852891000       0.838770000       2.327140000
C       -0.190395000       1.438306000       0.224005000
C        0.932819000       2.225096000       0.496186000
C        1.973938000       1.837688000       1.345251000
H        0.430335000      -0.492758000       3.308479000
H        2.591639000       0.803944000       3.107425000
H       -1.142704000       1.847182000      -0.051875000
H        0.918017000       3.247197000       0.158823000
H        2.828562000       2.485868000       1.409355000
```

4a (E$_h$ = -284.6380857; ZPVE = 0.095447)

```
N        0.006573000      -0.004774000       0.007084000
C        0.010873000      -0.001269000       1.254253000
C        0.699703000      -0.002131000       2.387835000
C        2.072014000      -0.506000000       2.225440000
C        1.075157000       0.777668000      -0.501221000
C        2.323266000       0.662513000      -0.003255000
C        2.776276000      -0.176974000       1.120017000
H        0.332784000       0.425916000       3.298757000
H        2.526441000      -1.113963000       2.987749000
H        0.862924000       1.377966000      -1.364612000
H        3.099850000       1.187241000      -0.531262000
H        3.792056000      -0.525072000       1.047050000
```

Optimized geometries (Cartesian coordinates, Å), electronic energies (E$_h$, in hartree) and zero-point vibrational energy (ZPVE, in hartree) computed at B3LYP/6-311+G(2d,p) level of theory for PES around **3a**.

3a (E$_h$ = -286.3584379; ZPVE = 0.091166)

N	-1.669727000	-0.446682000	-0.641616000
C	-0.748535000	-0.827171000	0.117707000
C	0.550665000	-1.416393000	0.213061000
C	1.508614000	-0.482969000	-0.032797000
C	-1.114929000	0.581660000	0.413551000
C	-0.016649000	1.459828000	0.055727000
C	1.205303000	0.919777000	-0.222374000
H	0.746595000	-2.454967000	0.439160000
H	2.548313000	-0.787881000	-0.071167000
H	-1.820709000	0.848436000	1.190251000
H	-0.123490000	2.537123000	0.136614000
H	2.030566000	1.575669000	-0.472792000

TS2 (E$_h$ = -286.3520986; ZPVE = 0.089649; i = 481.9 cm^{-1})

N	1.515526000	-0.646094000	0.623838000
C	0.557134000	-1.051349000	-0.043095000
C	-0.764700000	-1.322370000	-0.294452000
C	-1.559642000	-0.233688000	0.076121000
C	1.287176000	0.502477000	-0.329256000
C	0.256297000	1.412787000	-0.124830000
C	-1.043653000	1.056278000	0.260527000
H	-1.128324000	-2.228556000	-0.755253000
H	-2.633071000	-0.376368000	0.141026000
H	2.080211000	0.659410000	-1.049883000
H	0.421789000	2.433458000	-0.459667000
H	-1.744962000	1.849905000	0.486818000

4a (E$_h$ = -286.3697838; ZPVE = 0.091175)

N	-1.122056000	-1.089394000	-0.460328000
C	0.021028000	-1.310836000	-0.034356000
C	1.241291000	-0.995269000	0.346722000
C	1.564536000	0.351090000	-0.148073000
C	-1.589232000	0.115780000	0.145621000
C	-0.784317000	1.198432000	0.233175000
C	0.613152000	1.315826000	-0.175252000
H	1.862361000	-1.572522000	1.015668000
H	2.570314000	0.580150000	-0.489877000
H	-2.633765000	0.143727000	0.432158000
H	-1.258021000	2.118325000	0.561311000
H	0.914760000	2.305943000	-0.503985000

Optimized geometries (Cartesian coordinates, Å), electronic energies (E_h , in hartree) and zero-point vibrational energy (ZPVE, in hartree) computed at CASSCF(8,8)/6-311+G(2d,p) level of theory for PES around **3c**.

$^3A_2$-**2c** (E_h = -339.7160012; ZPVE = 0.112829)

C	-1.044904000	1.212304000	-0.025132000
C	0.333441000	1.221321000	0.002931000
C	1.059969000	-0.000080000	0.012722000
C	0.329208000	-1.218915000	-0.004421000
C	-1.049057000	-1.204967000	-0.032354000
C	-1.759315000	0.004982000	-0.049006000
H	-1.582337000	2.143755000	-0.025193000
H	0.873793000	2.148778000	0.018213000
H	0.866372000	-2.148298000	0.005300000
H	-1.589751000	-2.134510000	-0.037907000
N	2.390398000	-0.002459000	0.037229000
N	-3.160049000	0.007204000	-0.019031000
H	-3.571478000	0.826633000	-0.409006000
H	-3.574222000	-0.807662000	-0.415614000

$^1A_2$-**2c** (E_h = -339.689639; ZPVE = 0.112328)

C	-1.034849000	-0.907024000	-0.830223000
C	0.324099000	-0.901874000	-0.870249000
C	1.089016000	0.009063000	-0.009416000
C	0.320539000	0.902317000	0.866659000
C	-1.038286000	0.859805000	0.870585000
C	-1.758105000	-0.045986000	0.041893000
H	-1.582420000	-1.575286000	-1.471128000
H	0.866764000	-1.555757000	-1.524383000
H	0.860595000	1.581987000	1.496208000
H	-1.588549000	1.524616000	1.512764000
N	2.360719000	0.023178000	-0.021442000
N	-3.153454000	-0.021351000	0.013743000
H	-3.573684000	-0.875432000	-0.281262000
H	-3.575888000	0.301853000	0.856466000

TS1 (E_h = −339.6781048; ZPVE = 0.112051; i = 190.9 cm^{-1})

N	−0.007552000	−0.030200000	0.012579000
C	−0.004187000	−0.001218000	1.266133000
C	1.041553000	0.012419000	2.294807000
C	0.998760000	1.066166000	3.130145000
C	−1.244346000	0.714804000	1.502672000
C	−1.108494000	1.958088000	2.198601000
C	−0.019012000	2.124185000	3.002475000
H	1.803704000	−0.740770000	2.346467000
H	1.735300000	1.180318000	3.904598000
H	−2.158747000	0.368597000	1.074887000
H	−1.885409000	2.701534000	2.170530000
N	0.149833000	3.231927000	3.836268000
H	1.097612000	3.526075000	3.934710000
H	−0.432536000	4.006583000	3.605017000

3c (E_h = −339.6843096; ZPVE = 0.113858)

N	−2.068883000	−0.434350000	0.760555000
C	−1.521005000	0.321375000	−0.075395000
C	−0.724930000	1.537162000	−0.164205000
C	0.593021000	1.258850000	−0.146237000
C	−1.109111000	−0.995936000	−0.449817000
C	0.319244000	−1.212165000	−0.172179000
C	1.113444000	−0.122994000	−0.034347000
H	−1.129181000	2.527582000	−0.226777000
H	1.318003000	2.051078000	−0.189602000
H	−1.631936000	−1.571295000	−1.187806000
H	0.744537000	−2.200798000	−0.157613000
N	2.509741000	−0.207274000	0.116248000
H	2.827095000	−1.133368000	0.305509000
H	2.868534000	0.415675000	0.808965000

TS2 (E$_h$ = -339.6487888; ZPVE = 0.112113; i= 804.3 cm^{-1})

C	-0.760127000	1.561100000	-0.223168000
C	-1.586898000	0.484804000	0.012800000
C	-1.121553000	-1.170596000	-0.350796000
C	0.275705000	-1.174924000	-0.336048000
C	1.063578000	-0.074521000	0.028613000
C	0.582046000	1.246129000	-0.021586000
H	-1.098182000	2.488680000	-0.638038000
H	0.787046000	-2.004326000	-0.792412000
H	1.304367000	2.044175000	-0.028857000
N	-1.833652000	-0.497351000	0.738661000
H	-1.696800000	-1.810758000	-0.990946000
N	2.459424000	-0.297931000	0.147917000
H	2.968221000	0.533917000	0.355570000
H	2.676054000	-0.985905000	0.836591000

4c (E$_h$ = -339.6874302; ZPVE = 0.113946)

N	-1.835922000	-0.505782000	-0.581256000
C	-1.034360000	-1.412883000	0.154405000
C	0.265735000	-1.168567000	0.410680000
C	1.068073000	0.016552000	0.036851000
C	0.606861000	1.287603000	-0.026919000
C	-0.796733000	1.563080000	0.302273000
C	-1.640635000	0.664465000	-0.191717000
H	1.275701000	2.087096000	-0.296820000
H	-1.490707000	-2.345019000	0.426968000
H	0.825812000	-1.957151000	0.880683000
H	-1.106252000	2.352231000	0.957829000
N	2.432553000	-0.283436000	-0.149835000
H	2.581950000	-1.080333000	-0.731955000
H	2.961777000	0.487889000	-0.494625000

V. Rerefences

[1] Nunes, C. M.; Reva, I.; Kozuch, S.; McMahon, R. J.; Fausto, R. Photochemistry of 2-Formylphenylnitrene: A Doorway to Heavy-Atom Tunneling of a Benzazirine to a Cyclic Ketenimine. *J. Am. Chem. Soc.* **2017**, *139*, 17649-17659.

[2] Maltsev, A.; Bally, T.; Tsao, M. L.; Platz, M. S.; Kuhn, A.; Vosswinkel, M.; Wentrup, C. The Rearrangements of Naphthylnitrenes: UV/Vis and IR Spectra of Azirines, Cyclic Ketenimines, and Cyclic Nitrile Ylides. *J. Am Chem. Soc.* **2004**, 126, 237-249.

[3] Inui, H.; Sawada, K.; Oishi, S.; Ushida, K.; McMahon, R. J. Aryl Nitrene Rearrangements: Spectroscopic Observation of a Benzazirine and Its Ring Expansion to a Ketenimine by Heavy-Atom Tunneling. *J. Am. Chem. Soc.* **2013**, *135*, 10246-10249.

[4] Morawietz, J.; Sander, W. Photochemistry of Fluorinated Phenyl Nitrenes: Matrix Isolation of Fluorinated Azirines. *J. Org. Chem.* **1996**, *61*, 4351-4354.